Planck scale origin of nonzero θ_{13} and super-WIMP dark matter

Debasish Borah,[1,*] Biswajit Karmakar,[2,†] and Dibyendu Nanda[1,‡]
[1]*Department of Physics, Indian Institute of Technology Guwahati, Assam 781039, India*
[2]*Theoretical Physics Division, Physical Research Laboratory, Ahmedabad 380009, India*

(Received 26 June 2019; published 13 September 2019)

We study a discrete flavor symmetric scenario for neutrino mass and dark matter under the circumstances where such global discrete symmetries can be explicitly broken at the Planck scale, possibly by gravitational effects. Such explicit breaking of discrete symmetries mimic as Planck suppressed operators in the model, which can have nontrivial consequences for neutrino and dark matter sectors. In particular, we study a flavor symmetric model which, at a renormalizable level, gives rise to tri-bimaximal type neutrino mixing with vanishing reactor mixing angle $\theta_{13} = 0$, a stable inert scalar doublet behaving like a weakly interacting massive particle (WIMP) and a stable singlet inert fermion that does not interact with any other particles. The introduction of Planck suppressed operators that explicitly break the discrete symmetries can give rise to the generation of nonzero θ_{13} in agreement with neutrino data and also open up decay channels of inert scalar doublet into singlet neutral inert fermions leading to the realization of the super-WIMP dark matter scenario. We show that the correct neutrino phenomenology can be obtained in this model while discussing three distinct realizations of the super-WIMP dark matter scenario.

DOI: 10.1103/PhysRevD.100.055014

I. INTRODUCTION

Nonzero but tiny neutrino mass and large leptonic mixing have become a well-established fact by now, thanks to several experimental efforts in the last two decades [1–9]. For a review of neutrino mass and mixing, see Ref. [10]. Among these experiments, the relatively new ones, namely, the T2K [5], the Double Chooz [6], the Daya Bay [7], the RENO [8], and the MINOS [9] have not only reconfirmed the fact that neutrinos oscillate by making the measurements of mass squared differences and mixing angles more precise, but also discovered a nonzero value of reactor mixing angle θ_{13} which was thought to be almost vanishing earlier. For a recent global fit of neutrino oscillation data, we refer to Refs. [11,12]. Apart from neutrino oscillation experiments, a cosmology experiment like Planck also constrains the neutrino sector by putting an upper bound on the sum of absolute neutrino masses $\sum_i |m_i| < 0.11$ eV [13]. As indicated by these global fits, in spite of these experimental developments, there still remain several unknowns in the neutrino sector like the nature of neutrinos: Dirac or Majorana, mass hierarchy: normal or inverted, *CP* violating phases, etc. Apart from these, the origin of light neutrino mass also remains unknown in the standard model (SM) as the Higgs field does not have any renormalizable coupling to the neutrinos due to the absence of right-handed neutrinos. If we go beyond the renormalizable level, then it is possible to generate light neutrino mass of the Majorana type via a dimension five Weinberg operator [14] of type $(LLHH)/\Lambda$, where Λ is an unknown cutoff scale somewhere above the electroweak scale. Usual seesaw models [15–18] for light neutrino mass attempt to provide a dynamical origin of the Weinberg operator by introducing new fields like heavy right-handed neutrinos. Apart from the sub-eV mass, well below the electroweak scale, another puzzling feature related to neutrinos is their large mixing, in sharp contrast with small mixing angles in the quark sector. This has also motivated the study of different flavor symmetry models that can predict such large mixing patterns. One of the very popular flavor symmetric scenarios is the one that predicts a $\mu - \tau$ symmetric light neutrino mass matrix. However, such a scheme which predicts $\theta_{13} = 0, \theta_{23} = \frac{\pi}{4}$ and different values of θ_{12} depending upon the particular realization of this symmetry [19] has already been ruled out by recent neutrino experiments. Among such realizations, the tri-bimaximal (TBM) mixing [20–24], which predicts $\theta_{12} = 35.3°$, has been the most popular one. This mixing, which was consistent with neutrino data before the discovery of nonzero θ_{13}, can be realized naturally within several flavor symmetric

*dborah@iitg.ac.in
†biswajit@prl.res.in
‡dibyendu.nanda@iitg.ac.in

models based on non-Abelian discrete groups [25–28]. Among such flavor symmetric models, the discrete group A_4, a group of even permutations of four objects, can reproduce the TBM mixing in the most economical way [29–39]. However, in order to be consistent with the present neutrino data, such TBM or $\mu-\tau$ symmetric scenarios have to be corrected to generate a nonzero value of θ_{13}. There have been several attempts in that direction, some of which can be found in Refs. [40–62] and references therein.

Apart from nonzero neutrino mass and large leptonic mixing, another observed phenomena that has propelled a serious hunt for beyond standard model (BSM) physics is the presence of a nonbaryonic form of matter, or the so-called dark matter (DM) in large amounts in the present Universe. Apart from the long-standing astrophysical evidences [63–65], the recent cosmology experiment Planck suggests that almost 26% of the present Universe's energy density is in the form of DM while only around 5% is the usual baryonic matter leading the rest of the energy budget to mysterious dark energy [13]. In terms of the density parameter $\Omega_{\rm DM}$ and $h=$ Hubble parameter$/(100\ {\rm km\,s^{-1}\,Mpc^{-1}})$, the present DM abundance is conventionally reported as [13] $\Omega_{\rm DM}h^2=0.120\pm0.001$ at 68% C.L. Since none of the SM particles can satisfy the requirements for being a DM candidate, several BSM proposals have been put forward out of which the weakly interacting massive particle (WIMP) paradigm is perhaps the most popular or the most widely studied one. The coincidence is that a stable or cosmologically long-lived particle having electroweak scale mass and interactions fulfilling the criteria for observed DM abundance is often referred to as the *WIMP miracle*. However, if such particles having electroweak scale mass and interactions really exist in the Universe with such a large density, they are expected to pass through the detectors of several DM direct detection experiments giving rise to nuclear recoils. However, there has been no detection of particle DM at any experiments. The direct detection experiments like LUX [66], PandaX-II [67,68], and Xenon1T [69,70] have continued to produce null results so far. Similar null results follow from collider searches at the Large Hadron Collider (LHC) [71] as well as the indirect detection frontiers [72]. The typical indirect detection experiment's excess of antimatter, gamma rays, or neutrinos, originating perhaps from dark matter annihilations (for stable DM) or decay (for long-lived DM), and no convincing signal has been observed at any experiment operating in this frontier. Such null results from WIMP searches have led to the proposals of several alternative frameworks of DM, specially to scenarios where the interaction between DM and the visible sector could be much weaker than what it is in the WIMP paradigm. In fact, if the coupling of DM to the visible sector is sufficiently weak, then DM can never be produced thermally in the Universe requiring a nonthermal origin for its relic [73]. In such scenarios, the DM has a negligible initial number density in the early Universe and is produced from out of equilibrium decay or scattering of visible sector particles. The production mechanism for nonthermal DM is known as freeze-in and the candidates of nonthermal DM produced via freeze-in are often classified into a group called the freeze-in (feebly interacting) massive particle (FIMP). For a recent review of this DM paradigm, see Ref. [74]. The tiny couplings between DM and the visible sector can be naturally realized either by higher dimensional operators [73,75,76] or through some UV complete renormalizable theories [77]. While typical FIMP does not have many direct detection prospects and WIMP direct detection has so far failed, there exists a scenario which is a combination of both and has interesting detection prospects in terms of secondary particles. This is known as the super-WIMP scenario [78], where a metastable WIMP decays into a superweakly interacting dark matter at late epochs. Although DM still has feeble interactions with the visible sector, the metastable WIMP has sizable interactions and can be detected as, for example, a long-lived BSM particle at collider experiments [79]. This scenario was also adopted in the context of neutrino mass models in several works including Refs. [80–82]. In most such models there exists some exact or approximate discrete symmetries to stabilize the DM or to give rise to a long-lived metastable WIMP.

In this work, we try to find a common thread linking the discrete symmetries in the neutrino sector and DM sector. We consider the neutrino sector to have an exact $\mu-\tau$ symmetry while the dark sector has an exact Z_2 symmetry. We find a common source of breaking of these discrete symmetries through Planck scale suppressed operators by using the well-known argument that any generic theories of quantum gravity should not respect global symmetries: both discrete and continuous [83–85]. Recently, this argument was used to realize light neutrino mass from Planck scale lepton number breaking [86]. The effects of such Planck scale breaking of discrete symmetries on light neutrino parameters were studied within the context of the left-right symmetric model a few years back in Ref. [87]. Here we study the consequences of such Planck scale breaking of discrete symmetries on the neutrino sector, which generates nonzero θ_{13}, as required by the present neutrino data. At the same time, such breaking also makes it possible to realize the super-WIMP scenario by assisting the decay of a metastable WIMP to a superweakly interacting dark matter sector. We consider the presence of discrete flavor symmetries at a scale between the electroweak and Planck scale to dictate the patterns of neutrino mixing, neutrino mass, as well as DM dynamics while the Planck scale suppressed terms break these global discrete symmetries affecting the neutrino as well as the DM sector. The presence of an intermediate scale makes the Planck scale suppressed terms relevant in the discussion, which otherwise would have been of marginal importance through the usual Weinberg operator $(LLHH)/M_{\rm Pl}$ that remains several orders of magnitude below the typical neutrino mass scale, in the

absence of any intermediate scale between the electroweak scale and $M_{\rm Pl}$. We show that the scenario can have interesting predictions in both the neutrino and DM sectors. In the DM sector, we also discuss the corresponding phenomenology in the presence of a spontaneously broken gauged sector which forbids several Planck suppressed terms present in the scenario where the DM sector is charged only under some discrete global symmetries. Our framework can be generalized to a Planck scale origin of lepton number violation and hence neutrino mass, similar to Ref. [86] along with super-WIMP dark matter. We, however, restrict ourselves to discussing the origin of nonzero θ_{13} in this work, without assuming a global lepton number symmetry at the renormalizable level of the theory.

This paper is organized as follows. In Sec. II we discuss our flavor symmetric model and possible Planck suppressed operators. In Sec. III we discuss neutrino mass and mixing followed by super-WIMP dark matter phenomenology in Sec. IV. We finally conclude in Sec. V.

II. A_4 MODEL WITH TBM MIXING

In this section we outline the flavor model based on non-Abelian discrete group A_4 augmented by a Z_4 symmetry for the dark sector. A brief summary of the A_4 group, its representations and product rules are given in Appendix A. The particle content of the model, relevant for discussing the lepton sector and dark matter sector is shown in Table I. Apart from the SM lepton doublets and charged lepton singlets, there are three right-handed neutrinos required for implementing the type I seesaw mechanism [15–18]. In addition to the usual SM Higgs doublet, there exist three additional Higgs doublets required to generate Dirac mass terms for neutrinos. There also exist two more scalar fields responsible for generating the desired right-handed neutrino mass matrix and also to break the A_4 flavor symmetry spontaneously. Two more fields, one scalar and one fermion, both charged under the Z_4 symmetry, are included in order to achieve the desired DM phenomenology.

The renormalizable Yukawa Lagrangian for leptons can be written as

$$\begin{aligned}\mathcal{L}_Y \supset\ & Y_e\overline{L_e}He_R + Y_\mu\overline{L_\mu}H\mu_R + Y_\tau\overline{L_\tau}H\tau_R \\ & + (Y_{\nu 1}\overline{L_e} + Y_{\nu 2}\overline{L_\mu} + Y_{\nu 3}\overline{L_\tau})\tilde{H}_T N_R \\ & + (Y_\xi\xi + Y_N\phi_N)N_R N_R + \text{H.c.}, \end{aligned} \tag{1}$$

where $\tilde{H}_T = \tau_2 H_T^*$. Because of the additional Z_4 symmetry, the fields ψ, η do not have any renormalizable coupling with SM leptons or right-handed neutrinos. We assume ψ be vectorlike so that a bare mass term $M_\psi\bar{\psi}\psi$ is allowed in the Lagrangian. As mentioned earlier, gravity is not supposed to obey such global symmetries and hence we can write down Planck suppressed terms that explicitly break both A_4 and Z_4. The dimension five terms involving one of the A_4 triplet flavons ϕ_N, which explicitly break the discrete symmetries but preserve the gauge symmetries of the standard model, can be written as

$$\begin{aligned}\mathcal{L}_{\rm Planck} \supset \frac{1}{M_{\rm Pl}}\Bigg[& \sum_{i,\alpha,\beta}\phi_{Ni}(Y'_1\overline{L_\alpha}He_\beta + Y'_2\overline{L_\alpha}\eta e_\beta + Y''_1\overline{L_\alpha}\tilde{H}\psi \\ & + Y''_2\overline{L_\alpha}\tilde{\eta}\psi) + \sum_{i,\alpha,\beta}\phi_{Ni}(Y'_3\overline{L_\alpha}\tilde{H}N_\beta + Y'_4\overline{L_\alpha}\tilde{\eta}N_\beta) \\ & + \tilde{Y}_1 H\eta^\dagger\psi\psi\Bigg] + \text{H.c.} \end{aligned} \tag{2}$$

We can also write down the dimension five terms simultaneously involving two of the A_4 triplet flavons H_T, ϕ_N, which explicitly break the discrete symmetries but preserve the gauge symmetries of the standard model. They can be written as

$$\begin{aligned}\mathcal{L}_{\rm Planck} \supset \frac{1}{M_{\rm Pl}}\Bigg[& \sum_{i,j,\alpha,\beta}\phi_{Ni}(\tilde{Y'}_1\overline{L_\alpha}H_{Tj}e_\beta + \tilde{Y''}_1\overline{L_\alpha}\tilde{H}_{Tj}\psi \\ & + \tilde{Y'}_3\overline{L_\alpha}\tilde{H}_{Tj}N_\beta) + \tilde{Y}_2 H_{Tj}\eta^\dagger\psi\psi\Bigg] + \text{H.c.} \end{aligned} \tag{3}$$

One can prevent the coupling of η, ψ with standard model leptons at the dimension five level by considering an additional $U(1)_X$ gauge symmetry under which ψ is a Dirac fermion with charge n_1 while η has a charge $2n_1$. Thus, η can behave like a next to lightest particle that decays only to ψ due to the Planck scale effects on Z_2 symmetry breaking.

As discussed below, we choose a hierarchy of flavon vacuum expectation values (VEVs) in order to achieve the desired phenomenology. While the $SU(2)_L$ singlet flavon VEVs can be arbitrary, the same does not apply to that of the triplet flavon which is also a doublet under $SU(2)_L$. In order to be in agreement with precision electroweak measurements [10], the VEV of the neutral components of A_4 singlet Higgs doublet $H(v_1)$ and A_4 triplet Higgs doublet H_T, namely, v_i, $i = 2, 3, 4$ must satisfy $\sqrt{v_1^2 + v_2^2 + v_3^2 + v_4^2} \approx 174$ GeV. The scalar potential involving H, H_T only can be written as

TABLE I. Field content and transformation properties under $A_4 \times Z_4$ symmetry of the model.

Fields	L_e, L_μ, L_τ	e_R, μ_R, τ_R	H	H_T	ϕ_N	ξ	N_R	ψ	η
A_4	1, 1′, 1″	1, 1″, 1′	1	3	3	1	3	1	1
Z_4	1	1	1	1	1	1	1	i	−1
$SU(2)_L$	2	1	2	2	1	1	1	1	2
$U(1)_Y$	$\frac{1}{2}$	1	$-\frac{1}{2}$	$-\frac{1}{2}$	0	0	0	0	$-\frac{1}{2}$

$$
\begin{aligned}
V(H,H_T) = & -\mu_H^2 H^\dagger H - \mu_2^2 H_T^\dagger H_T + \lambda_1 (H^\dagger H)^2 + \lambda_2 [H_T^\dagger H]_1^2 + \lambda_3 [H_T^\dagger H_T]_{1'} [H_T^\dagger H_T]_{1''} \\
& + \frac{\lambda_4}{2} ([H_T^\dagger H_T^\dagger]_{1'} [H_T H_T]_{1''} + [H_T^\dagger H_T^\dagger]_{1''} [H_T H_T]_{1'}) + \lambda_5 [H_T^\dagger H_T^\dagger]_1 [H_T H_T]_1 \\
& + \frac{\lambda_6}{2} ([H_T^\dagger H_T]_{3_1} [H_T^\dagger H_T]_{3_1} + \text{H.c.}) + \lambda_7 [H_T^\dagger H_T]_{3_1} [H_T^\dagger H_T]_{3_2} + \lambda_8 [H_T^\dagger H_T^\dagger]_{3_1} [H_T H_T]_{3_2} \\
& + \lambda_9 [H_T^\dagger H_T]_1 H^\dagger H + \lambda_{10} [H_T^\dagger H]_{3_1} [H^\dagger H_T]_{3_1} + \frac{\lambda_{11}}{2} ([H_T^\dagger H_T^\dagger]_1 H H + \text{H.c.}) \\
& + \frac{\lambda_{12}}{2} ([H_T^\dagger H_T]_{3_1} H_T^\dagger H + \text{H.c.}) + \frac{\lambda_{13}}{2} ([H_T^\dagger H_T]_{3_2} [H_T^\dagger H]_{3_1} + \text{H.c.}) \\
& + \frac{\lambda_{14}}{2} ([H_T^\dagger H_T^\dagger]_{3_1} H_T H + \text{H.c.}) + \frac{\lambda_{15}}{2} ([H_T^\dagger H_T^\dagger]_{3_2} H_T H + \text{H.c.}),
\end{aligned} \tag{4}
$$

which is similar to the scalar potential of a multi-Higgs doublet model with additional complications due to the nontrivial A_4 transformations of A_4. Similarly, one can write the scalar potential involving $SU(2)_L$ singlet scalar fields as well as their interactions with H, H_T. Although a complete analysis of vacuum alignment[1] is beyond the scope of this work, it is possible to keep the VEVs of H, H_T around the electroweak scale by suitable choices of their bare mass squared terms and quartic couplings, while keeping their interaction with the singlet flavons (which acquire high scale VEVs) sufficiently small. The phenomenological and detection prospects of the components of H_T will be similar to two or multi-Higgs doublet models [90,91] as the physical masses of all the components can be kept around the TeV scale.

III. LEPTON MASSES AND MIXINGS

Up to leading order, owing to the A_4 symmetry, one can write the charged lepton mass matrix in the diagonal form as

$$
M_\ell = \begin{pmatrix} Y_e & 0 & 0 \\ 0 & Y_\mu & 0 \\ 0 & 0 & Y_\tau \end{pmatrix} v_1, \tag{5}
$$

where v_1 is the VEV of the neutral component of the Higgs doublet H. We use the A_4 product rules given in Appendix A in order to evaluate the forms of different mass matrices at the renormalizable level. Considering the vacuum alignment of the A_4 triplet scalar field $H_T = (v_2, 0, 0)$, the Dirac neutrino mass matrix at leading order can be written as,

$$
M_D^0 = \begin{pmatrix} Y_{\nu 1} v_2 & 0 & 0 \\ 0 & 0 & Y_{\nu 2} v_2 \\ 0 & Y_{\nu 3} v_2 & 0 \end{pmatrix}, \tag{6}
$$

where, without any loss of generality, one can consider $Y_{\nu 1} = Y_{\nu 2} = Y_{\nu 3}$.

Considering triplet flavon vacuum alignment as $\langle \phi_N \rangle = u(1,1,1)$ and $\langle \xi \rangle = u_\xi$ the right-handed neutrino mass matrix at leading order is given by

$$
M_R = \begin{pmatrix} a + \frac{2b}{3} & -\frac{b}{3} & -\frac{b}{3} \\ -\frac{b}{3} & \frac{2b}{3} & a - \frac{b}{3} \\ -\frac{b}{3} & a - \frac{b}{3} & \frac{2b}{3} \end{pmatrix}, \tag{7}
$$

where $a = 2 Y_\xi u_\xi$ and $b = 2 Y_N u$. Hence the light neutrino mass matrix, using the type I seesaw formula is

$$
\begin{aligned}
-M_\nu &= M_D^0 M_R^{-1} M_D^{0T} \\
&= v_2^2 Y_{\nu 1}^2 \begin{pmatrix} \frac{3a+b}{3(a+b)} & \frac{b}{3(a+b)} & \frac{b}{3(a+b)} \\ \frac{b}{3(a+b)} & \frac{-b(2a+b)}{3(a+b)(a-b)} & \frac{3a^2+ab-b^2}{3(a+b)(a-b)} \\ \frac{b}{3(a+b)} & \frac{3a^2+ab-b^2}{3(a+b)(a-b)} & \frac{-b(2a+b}{3(a+b)(a-b)} \end{pmatrix}.
\end{aligned} \tag{8}
$$

This $\mu - \tau$ symmetric light neutrino mass matrix can be diagonalized by the usual tri-bimaximal mixing matrix given by [92]

$$
U_{\text{TBM}} = \begin{pmatrix} \sqrt{\frac{2}{3}} & \frac{1}{\sqrt{3}} & 0 \\ \frac{-1}{\sqrt{6}} & \frac{1}{\sqrt{3}} & \frac{-1}{\sqrt{2}} \\ \frac{-1}{\sqrt{6}} & \frac{1}{\sqrt{3}} & \frac{1}{\sqrt{2}} \end{pmatrix}, \tag{9}
$$

predicting $\theta_{13} = 0$ and maximal value of θ_{23}. Present experimental observation, however, rules out the $\theta_{13} = 0$ scenario and has a preference towards higher octant for θ_{23} (i.e., $\theta_{23} > 45°$) [12]. We therefore consider the Planck scale suppressed corrections to such scenarios so that the correct light neutrino phenomenology can be obtained along with the implications for the dark sector.

The contribution to the light neutrino mass matrix and neutrino mixing from the Planck suppressed terms that

[1]For details of vacuum alignment in supersymmetric and nonsupersymmetric discrete flavor symmetric models, one may refer to Refs. [39,88] and Ref. [89], respectively.

break the discrete symmetries explicitly can arise in a variety of ways. For example,

(i) there can be contributions to light neutrino mass matrix of the type $(LLHH)/M_{\rm Pl}$, $(LLH_TH_T)/M_{\rm Pl}$, $(LLH_TH)/M_{\rm Pl}$, all of which remain at least 10^{-5} times smaller than the typical neutrino mass scale, in the absence of any intermediate scale between the electroweak scale and $M_{\rm Pl}$.

(ii) there can be new contributions to charged lepton mass matrix of the type $\phi_{Ni}(Y'_1\overline{L_\alpha}He_\beta)/M_{\rm Pl}$, which can be suppressed by an additional factor $u/M_{\rm Pl}$ compared to the leading order contributions to charged lepton masses. But such corrections can, in principle, lead to deviations from diagonal charged lepton mass matrix. Usually, the leptonic mixing matrix is given in terms of the charged lepton diagonalizing matrix (U_l) and light neutrino diagonalizing matrix U_ν as $U = U_l^\dagger U_\nu$. In the simple case where the charged lepton mass matrix is diagonal, which is true in our model at tree level, we can have $U_l = \mathbb{1}$. Therefore we can write $U = U_\nu$. But U_l may become nontrivial after the corrections are added and it will mimic as a correction in the leading order leptonic mixing, which is TBM type.

(iii) there can be corrections to the Dirac neutrino mass matrix of the type $\phi_{Ni}(Y'_3\overline{L_\alpha}\tilde{H}N_\beta)/M_{\rm Pl}$, which can again be suppressed by an additional factor $u/M_{\rm Pl}$ compared to the leading order contributions. Such corrections will propagate to the light neutrino mass matrix through the type I seesaw formula.

(iv) there can be corrections to the right-handed neutrino mass matrix of the type $(Y'_\xi\xi^2 + Y'_N\phi_N^2)N_RN_R/M_{\rm Pl}$, which can change the structure of M_R from the $\mu-\tau$ symmetric leading order form mentioned before. Once again this correction will propagate to the light neutrino mass matrix via the type I seesaw formula.

All these corrections can be simultaneously or separately sufficient to generate correct neutrino mixing. For representative purposes, we will consider corrections to the Dirac neutrino mass matrix only and that too via the Higgs doublet H. Addition of other corrections will make the calculations complicated without any new insights. A more general analysis is beyond the scope of this work and left for future studies.

Now, following Eq. (2), the correction to the Dirac neutrino mass matrix now can be written as

$$M_D^1 = \frac{uv_1}{M_{\rm Pl}}\begin{pmatrix}(Y'_3)_{11} & (Y'_3)_{12} & (Y'_3)_{13}\\ (Y'_3)_{21} & (Y'_3)_{22} & (Y'_3)_{23}\\ (Y'_3)_{31} & (Y'_3)_{32} & (Y'_3)_{33}\end{pmatrix}, \tag{10}$$

In the present construction, following A_4 multiplication rules given in the Appendix, we find that $(Y'_3)_{11} = (Y'_3)_{23} = (Y'_3)_{32}$, $(Y'_3)_{12} = (Y'_3)_{21} = (Y'_3)_{33}$, and $(Y'_3)_{13} = (Y'_3)_{22} = (Y'_3)_{31}$. With such correction, the effective Dirac neutrino mass matrix can be written as (assuming $Y_{\nu1} = Y_{\nu2} = Y_{\nu3}$)

$$\begin{aligned} M_D = M_D^0 + M_D^1 &= \begin{pmatrix} Y_{\nu1}v_2 & 0 & 0\\ 0 & 0 & Y_{\nu1}v_2\\ 0 & Y_{\nu1}v_2 & 0\end{pmatrix}\\ &\quad + \frac{uv_1}{M_{\rm Pl}}\begin{pmatrix}(Y'_3)_{11} & (Y'_3)_{12} & (Y'_3)_{13}\\ (Y'_3)_{12} & (Y'_3)_{13} & (Y'_3)_{11}\\ (Y'_3)_{13} & (Y'_3)_{11} & (Y'_3)_{12}\end{pmatrix},\\ &= v\begin{pmatrix} y_1 & y_2 & y_3\\ y_2 & y_3 & y_1\\ y_3 & y_1 & y_2\end{pmatrix}, \end{aligned} \tag{11}$$

where $y_1 = Y_{\nu1} + \frac{u}{M_{\rm Pl}}(Y'_3)_{11}$, $y_2 = \frac{u}{M_{\rm Pl}}(Y'_3)_{12}$, and $y_3 = \frac{u}{M_{\rm Pl}}(Y'_3)_{13}$ with $v = v_2 = v_1$.

Now, along with the Planck suppressed operator contribution in Dirac neutrino mass, the light neutrino mass originating from type I seesaw can be written as

$$-M_\nu = M_D M_R^{-1} M_D^T. \tag{12}$$

After a rotation by $U_{\rm TBM}$, the light neutrino mass matrix can be written as

$$\begin{aligned} M'_\nu &= U_{\rm TBM}^T M_\nu U_{\rm TBM}\\ &= \begin{pmatrix} \frac{-v^2(ax_2+2bx_3)}{a^2-b^2} & 0 & \frac{-\sqrt{3}v^2x_1}{a^2-b^2}\\ 0 & \frac{v^2x_4}{a} & 0\\ \frac{-\sqrt{3}v^2x_1}{a^2-b^2} & 0 & \frac{v^2(ax_2-2bx_3)}{a^2-b^2}\end{pmatrix}, \end{aligned} \tag{13}$$

where

$$x_1 = (2y_1 - y_2 - y_3)(y_2 - y_3), \tag{14}$$

$$x_2 = -2y_1^2 + y_2^2 - 4y_2y_3 + y_3^2 + 2y_1(y_2 + y_3), \tag{15}$$

$$x_3 = y_1^2 + y_2^2 - y_2y_3 + y_3^2 - y_1(y_2 + y_3), \tag{16}$$

$$x_4 = (y_1 + y_2 + y_3)^2. \tag{17}$$

Clearly an additional rotation in the 13 plane is required to diagonalize the above matrix via the relation

$$U_{13}^T M'_\nu U_{13} = {\rm diag}(m_1e^{i\gamma_1}, m_2e^{i\gamma_2}, m_3e^{i\gamma_3}) \tag{18}$$

with

$$U_{13} = \begin{pmatrix}\cos\theta & 0 & \sin\theta e^{-i\psi}\\ 0 & 1 & 0\\ -\sin\theta e^{i\psi} & 0 & \cos\theta\end{pmatrix}, \tag{19}$$

where m_1, m_2, m_3 are the real positive neutrino mass eigenvalues and $\gamma_{1,2,3}$ are the respective Majorana phases. Therefore the effective neutrino mixing matrix (with diagonal charged lepton sector) can be written as

$$U_\nu = U_{\rm TBM} U_{13} U_m, \tag{20}$$

where U_m is the diagonal Majorana phase matrix given by $U_m = \mathrm{diag}(e^{i\gamma_1}, e^{i\gamma_2}, e^{i\gamma_3})$. Comparing this with the Pontecorvo-Maki-Nakagawa-Sakata (PMNS) mixing matrix

$$U_{\rm PMNS} = \begin{pmatrix} c_{12}c_{13} & s_{12}c_{13} & s_{13}e^{-i\delta} \\ -s_{12}c_{23} - c_{12}s_{23}s_{13}e^{i\delta} & c_{12}c_{23} - s_{12}s_{23}s_{13}e^{i\delta} & s_{23}c_{13} \\ s_{12}s_{23} - c_{12}c_{23}s_{13}e^{i\delta} & -c_{12}s_{23} - s_{12}c_{23}s_{13}e^{i\delta} & c_{23}c_{13} \end{pmatrix} P, \tag{21}$$

one can obtain the correlation between the model parameters and neutrino oscillation parameters. In the above PMNS mixing matrix, $P(= \mathrm{diag}(1, e^{i\alpha_{21}/2}, e^{i\alpha_{31}/2}))$ is the Majorana phase matrix where $\alpha_{21} = (\gamma_1 - \gamma_2)$ and $\alpha_{31} = (\gamma_1 - \gamma_3)$ are the physical Majorana phases after rotating away one common phase that is irrelevant. The rotation parameter θ in the rotation matrix (19) can be obtained as

$$\tan 2\theta = \pm\sqrt{3}\frac{x_1}{x_2}, \tag{22}$$

with $\psi = 0, \pi$, respectively, yielding maximal value for the Dirac CP phase δ. The construction of the present setup is such that we have considered the Planck scale suppressed terms only for the Dirac neutrino mass matrix. Once we allow correction terms for the charged lepton and/or right-handed neutrino mass matrix, nonmaximal values for the Dirac CP phase δ become allowed [54,93,94]. Comparing the neutrino mixing matrix of our scenario given in Eq. (20) with the standard parametric form of mixing matrix given in Eq. (21), the neutrino mixing angles can be evaluated as [54]

$$\sin^2\theta_{13} = \frac{2}{3}|\sin\theta|^2, \tag{23}$$

$$\sin^2\theta_{12} = \frac{1}{3(1-\sin^2\theta_{13})}, \tag{24}$$

$$\sin^2\theta_{23} = \frac{1}{2} + \frac{1}{\sqrt{2}}\sin\theta_{13}\sin\psi. \tag{25}$$

Thus, the neutrino mixing angles are a function of the angle θ, which depends upon $x_{1,2}$, and they further depend upon the coupling constants $y_{1,2,3}$ as described before. As mentioned earlier, in the present setup we have considered the deviation from TBM mixing (which usually predicts $\sin^2\theta_{12} = 1/3$, $\sin^2\theta_{23} = 1/2$ and $\theta_{13} = 0$) via Planck scale suppressed operators appearing solely in the neutrino sector. The present construction (based on A_4 discrete symmetry) is such that observed θ_{13} can be successfully generated in the presence of such operators and deviations in θ_{12} and θ_{23} from their respective TBM values also arise at the same time. Such deviation from TBM mixing can be obtained via a unitary rotation (in the 13 plane) matrix, U_{13}, parametrized only by two parameters θ and ψ, which also satisfy the condition $|(U_{13})_{11}|^2 + |(U_{13})_{13}|^2 = 1$. The correlations among θ, ψ, and the mixing angles are generic features of this class of models [42,53,95] considered here and can be realized very easily using A_4 discrete symmetry [54,93,94,96]. However, in contrast to all other models mentioned above, the present scenario predicts the Dirac CP phase δ to be maximal (as ψ acquires values 0 and π). Such predictions naturally make the model testable as well as distinguishable from other scenarios. Now, the neutrino mass eigenvalues can be written as

$$m_1 = v^2 x_3/|a|\sqrt{1+\alpha^2+2\alpha\cos\phi_{ba}}, \tag{26}$$

$$m_2 = v^2 x_4/|a|, \tag{27}$$

$$m_3 = v^2 x_3/|a|\sqrt{1+\alpha^2-2\alpha\cos\phi_{ba}}, \tag{28}$$

where $\alpha = |b|/|a|$ and $\phi_{ba} = \phi_b - \phi_a$ is the phase difference between b and a. Using these, one can now define a ratio of solar to atmospheric mass-squared differences ($\Delta m^2_\odot = \Delta m^2_{21} = m_2^2 - m_1^2$ and $|\Delta m^2_A| = |\Delta m^2_{31}| = m_3^2 - m_1^2 \approx |\Delta m^2_{32}| = m_3^2 - m_2^2$, respectively) defined by

$$r = \frac{\Delta m^2_\odot}{|\Delta m^2_A|} = \frac{(x_4^2(\alpha^2 + 2\alpha\cos\phi_{ba}) - x_3^2)(1+\alpha^2-2\alpha\cos\phi_{ba})}{\pm x_3^2 4\alpha\cos\phi_{ba}}. \tag{29}$$

Here, depending on the sign of denominator, the parameter space is divided into two parts: "+" in the denominator yields normal hierarchy of neutrino mass whereas for "−" in the denominator yields inverted neutrino mass hierarchy. Therefore, the neutrino mixing angles and the ratio of solar to atmospheric mass-squared differences are altogether functions of five parameters, namely, three coupling

constants y_1, y_2, y_3 and α, ϕ_{ba}. Using the observed neutrino oscillation data summarized in the latest global fit [12], these parameters can be constrained for both normal and inverted neutrino mass hierarchy, as we discuss below.

A. Normal hierarchy

Here we first explore neutrino phenomenology for normal neutrino mass hierarchy. In the left panel (right panel) of Fig. 1 we have shown the allowed points for y_1 vs y_2 (y_3). All these points satisfy the 3σ allowed range for the three neutrino mixing angles, the ratio of solar to atmospheric mass-squared differences [12]. From Eqs. (26) and (27), one can easily obtain the common factor $|a|$ appearing in the absolute neutrino mass using $\Delta m^2_{21} = m_2^2 - m_1^2 = 2.43 \times 10^{-5}$ eV^2. Therefore the parameter space can be further constrained using the cosmological upper limit on the sum of absolute neutrino masses $\sum_i |m_i| < 0.11$ eV [13]. The allowed regions presented in Fig. 1 also satisfy this constraint. Now, in the left panel of Fig. 2 we have plotted the allowed regions in the α-ϕ_{ba} plane. As mentioned earlier here α is the ratio of the two parameters appearing in the right-handed neutrino mass matrix and ϕ_{ba} is their relative phase difference. This complex phase factor plays a crucial role in the present analysis in determination of the neutrino masses and the associated (Majorana) phases. In the right panel of Fig. 2 we have shown the predictions for the Majorana phases in the current setup. Predictions for the Majorana phases are also important to evaluate the absolute neutrino mass parameter ($m_{\beta\beta}$) appearing in the neutrinoless double beta decay amplitude, which is shown in the right panel of Fig. 3. In this figure the gray band represents the standard light neutrino contribution to $m_{\beta\beta}$ for a 3σ range of neutrino oscillation parameters in the case of normal hierarchy and the dark red points superimposed over the gray band are the predicted regions in our setup. Here we find that the predicted region entirely falls inside the correct allowed region for $m_{\beta\beta}$ in the standard three neutrino picture. In the left panel of Fig. 3 we present the prediction regarding the sum of absolute neutrino masses as a function of the lightest light neutrino m_1 for normal hierarchy. As can be seen here, there are enough points lying within the cosmological upper

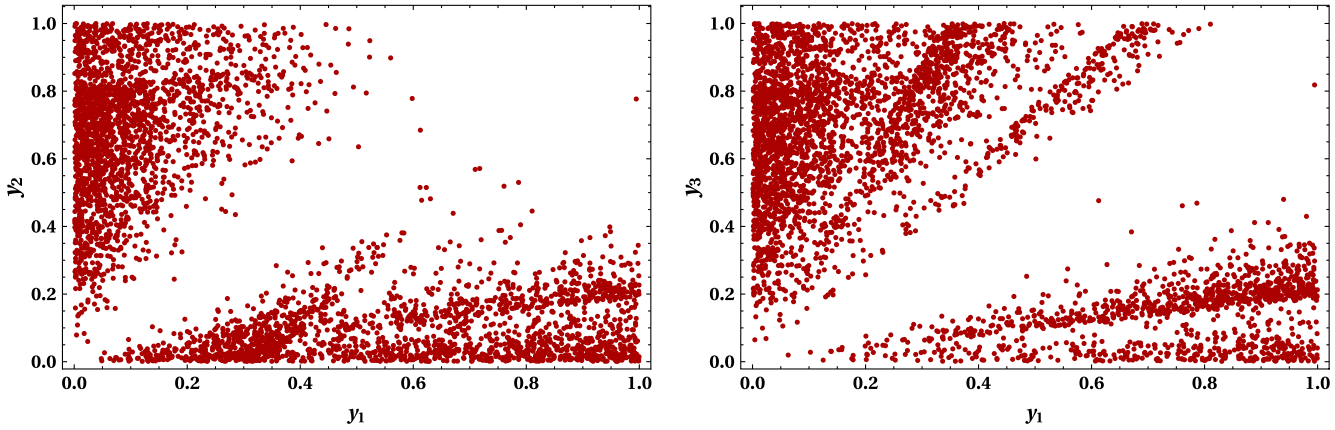

FIG. 1. y_1 vs y_2 and y_1 vs y_3 satisfying correct neutrino data for normal hierarchy.

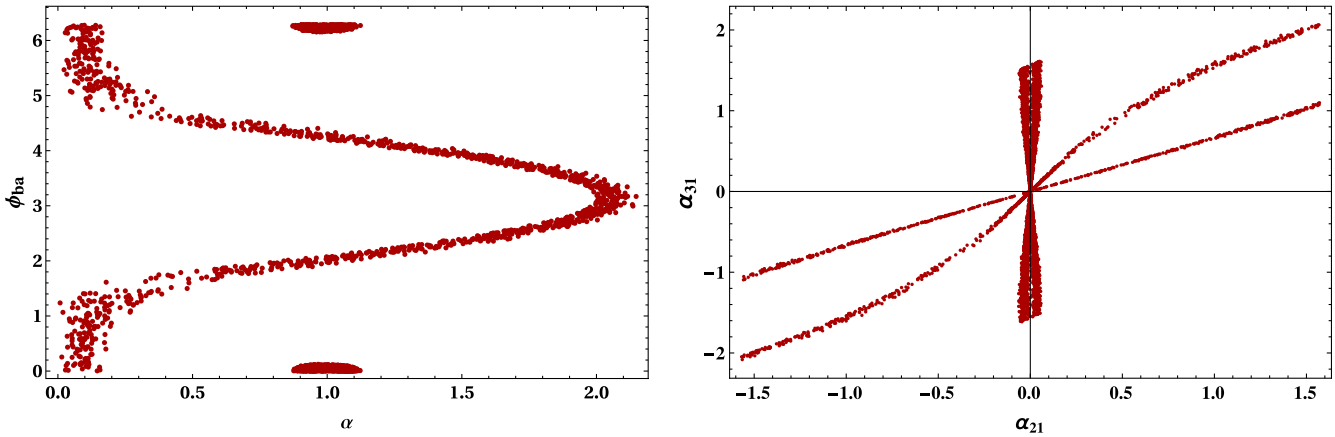

FIG. 2. Left panel represents α vs ϕ_{ba} satisfying correct neutrino data. Right panel represents predicted regions for the Majorana phases α_{21} and α_{31} for normal hierarchy.

bound on the sum of the absolute neutrino masses mentioned earlier.

B. Inverted hierarchy

Using a similar strategy, we analyze the allowed parameter space for inverted neutrino mass hierarchy. In Fig. 4, the blue dots in left panel (right panel) represent allowed points for y_1 vs y_2 (y_3) satisfying the correct neutrino oscillation data. In Fig. 5, the left panel shows the allowed points in the α-ϕ_{ba} plane whereas the right panel shows the predictions for the two Majorana phases α_{21} and α_{31} for inverted neutrino mass hierarchy. Finally, in Fig. 6 we show the predictions for the absolute neutrino masses (left panel) and $m_{\beta\beta}$ as a function of lightest neutrino mass m_3. Interestingly, for values $y_{1,2,3} \leq 1$, we find that the predictions for the effective neutrino mass parameter $m_{\beta\beta}$ mostly fall outside of the standard allowed regions (shown as a gray colored band) for inverted hierarchy. This makes the inverted hierarchy in the current scenario less favorable compared to the normal hierarchy. However, such conclusions are based on the very specific Planck suppressed corrections we have considered in our analysis and they will change if more corrections are included. However, the essence of the setup is that the correct light neutrino phenomenology can be obtained for different subsets of the entire parameter space.

It should be noted that the Planck scale suppressed corrections crucially depend upon the ratio $u/M_{\rm Pl}$ up to some Yukawa couplings. In the absence of any fine-tuning of Yukawa couplings, all the corrections to the neutrino sector go as $M_R/M_{\rm Pl}$ since $M_R \propto u$. In fact, the usual Weinberg operator $(LLHH)/M_{\rm Pl}$ can give a correction like $\frac{M_R}{M_{\rm Pl}} M_\nu$, where M_ν is the leading order type I seesaw contribution to light neutrino mass. For example, if the scale of A_4 breaking at the renormalizable level is $u \sim 10^{16}$ GeV, similar to the typical grand unified theory (GUT) scale, one can have a slightly lower scale $M_R \sim 10^{14}$ GeV and hence the scale a, b in the right-handed neutrino mass matrix given in Eq. (7), by appropriate tuning of relevant Yukawa couplings. Such M_R can generate sub-eV scale light neutrino mass matrix at leading order for order one Dirac Yukawa couplings. If we consider the corrections to Dirac neutrino mass matrix, such a scale would correspond to y_2, $y_3 \leq 10^{-3}$–10^{-2} which will correspond to the lowermost regions (along the y axis) of the parameter space shown in

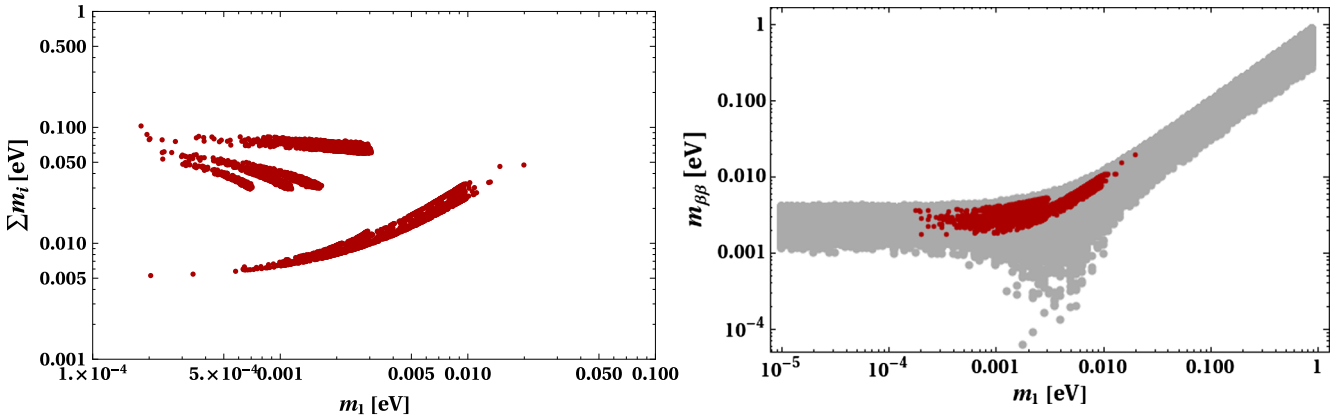

FIG. 3. Predictions for lightest neutrino mass (m_1 for normal hierarchy) vs sum of absolute neutrino masses (left panel). Predictions for lightest neutrino mass (m_1 for normal hierarchy) vs effective mass parameter for neutrinoless double beta decay (right panel).

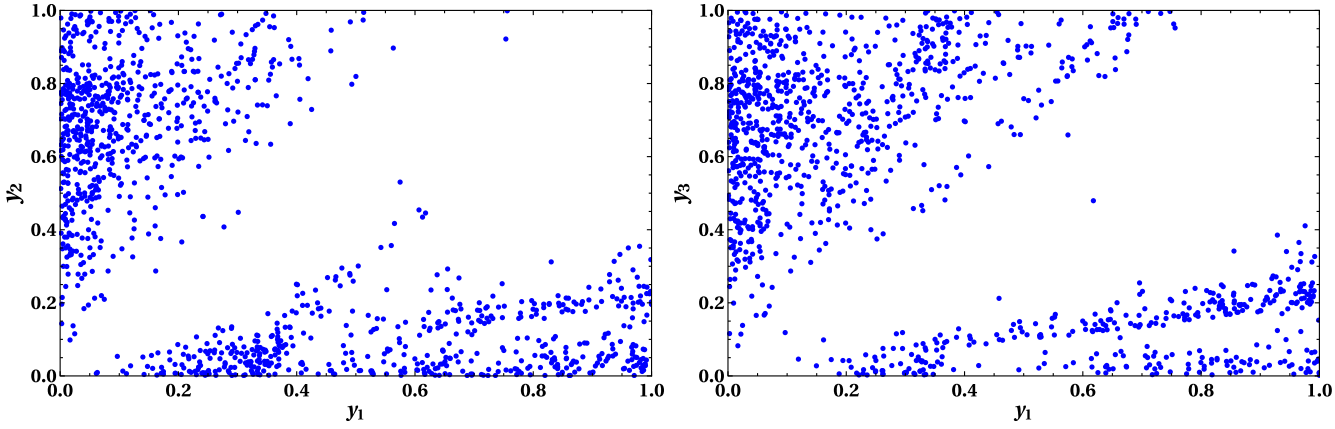

FIG. 4. y_1 vs y_2 and y_1 vs y_3 satisfying correct neutrino data for inverted hierarchy.

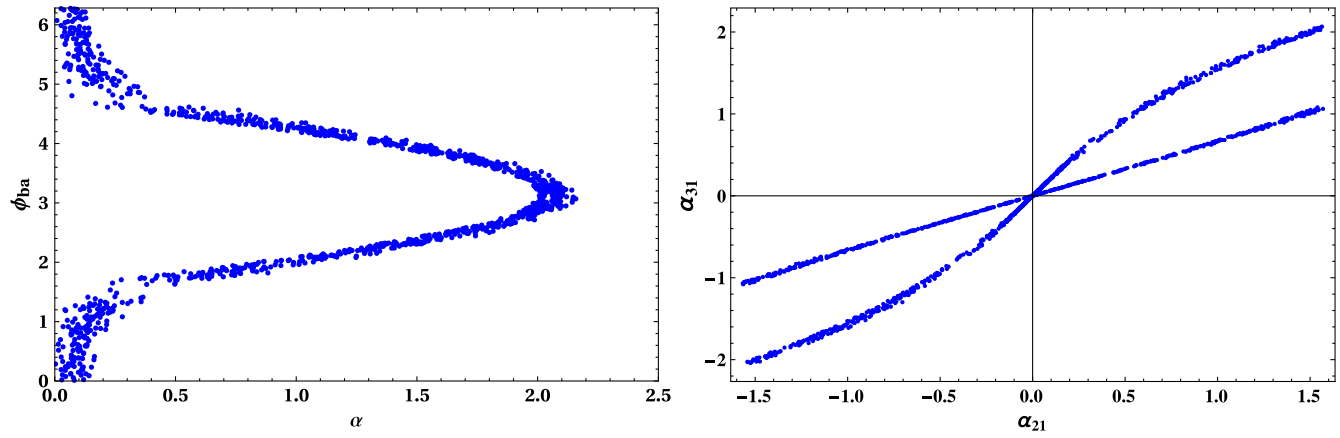

FIG. 5. Left panel represents α vs ϕ_{ba} satisfying the correct neutrino data. Right panel represents the predicted regions for the Majorana phases α_{21} and α_{31} for inverted hierarchy.

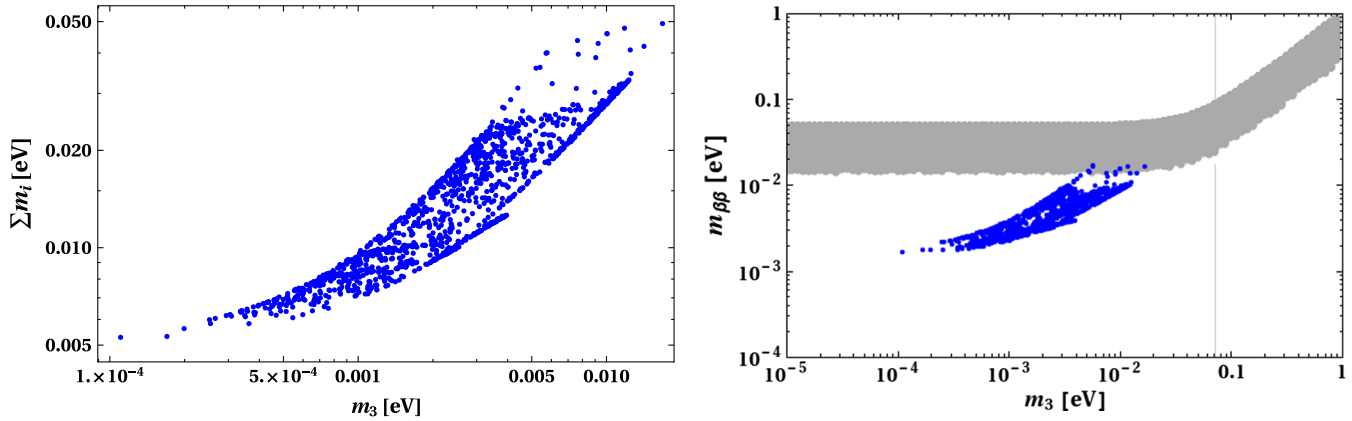

FIG. 6. Predictions for lightest neutrino mass (m_3 for inverted hierarchy) vs sum of absolute neutrino masses (left panel). Predictions for lightest neutrino mass (m_3 for inverted hierarchy) vs effective mass parameter for neutrinoless double beta decay (right panel).

Figs. 1 and 4 described before. Similar estimates about these couplings can be made for different symmetry breaking scale. However, in order to have sizable corrections to the TBM mixing and to avoid unnaturally fine-tuned as well as nonperturbative Yukawa couplings, the A_4 scale should be close to the GUT scale. As far as fine-tuning is concerned, we set a tolerance the same as the electron Yukawa in the standard model. A different A_4 breaking scale will also have different implications for the super-WIMP dark matter sector, requiring some amount of fine-tuning in relevant Yukawa couplings related to the mother particle and dark matter, as we discuss below.

IV. SUPER-WIMP DARK MATTER

The dark matter in our setup is similar to the super-WIMP scenario [78], where a metastable WIMP decays into superweakly interacting dark matter at late epochs. As can be seen from the dimension five Lagrangian (2), there are several terms which can give rise to decay of either ψ or η, the particles of the Z_4 sector. At the renormalizable level however, both of them are stable due to the unbroken Z_4 symmetry. While η can be produced thermally in the early Universe due to its electroweak gauge interactions, the singlet fermion ψ has negligible thermal abundance. In a general super-WIMP formalism where η is the metastable WIMP and ψ is the DM candidate, one can write down the decay width of η into two dark matter particles (ψ) as

$$\Gamma_{\eta\to\psi\bar{\psi}} = \frac{Y_{\eta\psi}^2(m_\eta^2 - 4m_\psi^2)}{8\pi m_\eta}\sqrt{1-\frac{4m_\psi^2}{m_\eta^2}}, \tag{30}$$

where $Y_{\eta\psi}$ is the effective Yukawa coupling and m_η and m_ψ are the masses of the mother particle η and ψ, respectively.

However, this doublet scalar, apart from having electroweak gauge interactions, can have sizeable quartic interactions with other scalars like the standard model Higgs doublet and hence can be thermally produced in the early Universe. Now, considering the mother particle η to be in thermal equilibrium in the early Universe which also decays into the dark matter particle ψ, we can write down the relevant Boltzmann equations for comoving number densities of η, ψ as

$$\frac{dY_\eta}{dx} = -\frac{4\pi^2}{45}\frac{M_{\rm Pl}M_{\rm sc}}{1.66}\frac{\sqrt{g_\star(x)}}{x^2} \times \left[\sum_{p=\text{SM particles}} \langle\sigma v\rangle_{\eta\eta\to p\bar{p}}(Y_\eta^2 - (Y_\eta^{\rm eq})^2)\right] - \frac{M_{\rm Pl}}{1.66}\frac{x\sqrt{g_\star(x)}}{M_{\rm sc}^2 g_s(x)}\Gamma_{\eta\to\bar{\psi}\psi}Y_\eta, \quad (31)$$

$$\frac{dY_\psi}{dx} = \frac{2M_{\rm Pl}}{1.66}\frac{x\sqrt{g_\star(x)}}{M_{\rm sc}^2 g_s(x)}\Gamma_{\eta\to\bar{\psi}\psi}Y_\eta, \quad (32)$$

where $x = \frac{M_{\rm sc}}{T}$ is a dimensionless variable, while $M_{\rm sc}$ is some arbitrary mass scale which we choose equal to the mass of η, and $M_{\rm Pl}$ is the Planck mass. Moreover, $g_s(x)$ is the number of effective degrees of freedom associated to the entropy density of the Universe and the quantity $g_\star(x)$ is defined as

$$\sqrt{g_\star(x)} = \frac{g_{\rm s}(x)}{\sqrt{g_\rho(x)}}\left(1 - \frac{1}{3}\frac{{\rm d}\ln g_{\rm s}(x)}{{\rm d}\ln x}\right). \quad (33)$$

Here, $g_\rho(x)$ denotes the effective number of degrees of freedom related to the energy density of the universe at $x = \frac{M_{\rm sc}}{T}$. The first term on the right-hand side of the Boltzmann equation (31) corresponds to the self annihilation of η into standard model particles and vice versa, which play the role in its freeze-out. The second term on the right-hand side of this equation corresponds to the dilution of η due to its decay into dark matter ψ. Let us denote the freeze-out temperature of η as T_F and its decay temperature as T_D. If we assume that the mother particle freezes out first followed by its decay into dark matter particles, we can consider $T_F > T_D$. In such a case, we can first solve the Boltzmann equation for η considering only the self-annihilation part to calculate its freeze-out abundance.

$$\frac{dY_\eta}{dx} = -\frac{4\pi^2}{45}\frac{M_{\rm Pl}M_{\rm sc}}{1.66}\frac{\sqrt{g_\star(x)}}{x^2} \times \left[\sum_{p=\text{SM particles}} \langle\sigma v\rangle_{\eta\eta\to p\bar{p}}(Y_\eta^2 - (Y_\eta^{\rm eq})^2)\right]. \quad (34)$$

Then we solve the following two equations for temperature $T < T_F$:

$$\frac{dY_\eta}{dx} = -\frac{M_{\rm Pl}}{1.66}\frac{x\sqrt{g_\star(x)}}{M_{\rm sc}^2 g_s(x)}\Gamma_{\eta\to\bar{\psi}\psi}Y_\eta, \quad (35)$$

$$\frac{dY_\psi}{dx} = \frac{2M_{\rm Pl}}{1.66}\frac{x\sqrt{g_\star(x)}}{M_{\rm sc}^2 g_s(x)}\Gamma_{\eta\to\bar{\psi}\psi}Y_\eta. \quad (36)$$

We stick to this simplified assumption $T_F > T_D$ in this work and postpone a more general analysis without any assumption to an upcoming work. The assumption $T_F > T_D$ allows us to solve the Boltzmann equation (34) for η first, calculate its freeze-out abundance, and then solve the corresponding equations (35), (36) for η, ψ using the freeze-out abundance of η as the initial condition.[2] In such a scenario, we can solve the Boltzmann equations (35), (36) for different benchmark choices of $Y, m_\eta, m_{\rm DM} \equiv M_\psi$ and estimate the freeze-out abundance of η that can generate $\Omega h^2 = 0.12$, the *canonical* value of the dark matter (ψ) relic abundance in the present Universe. This required freeze-out abundance of η then restricts the parameters involved in its coupling to the SM particles. It turns out that a scalar singlet like η interacts with the SM particles only through the Higgs portal and hence depends upon the $\eta - H$ coupling, denoted by $\lambda_{H\eta}$. To find out the freeze-out abundance of η, we have used the micrOMEGAs package [98] in our work.

Now, as can be seen from the Planck suppressed terms of Eq. (2), there are three different decay modes of η, namely, $\eta \to l\bar{l}, l\psi, \psi\psi$, where l denotes a SM lepton. Out of these, the decay mode $\eta \to \psi\psi$ has effective coupling $\tilde{Y}_1\frac{v}{M_{\rm Pl}}$, where v is the Higgs VEV at the electroweak scale. The other two decay modes have larger effective coupling $\tilde{Y}'_2\frac{v_\phi}{M_{\rm Pl}}, \tilde{Y}''_2\frac{v_\phi}{M_{\rm Pl}}$ where v_ϕ is the A_4 flavon VEV. Since the flavon VEV is much larger than the electroweak one, the first two decay modes will be more dominant than the last one. Out of these two, the mode $\eta \to l\psi$ will contribute to the abundance of DM ψ. One can also think of some nonminimal scenarios where there exists some local symmetries which forbid $\eta \to l\bar{l}$ or even $\eta \to l\psi$, depending upon how η, ψ are charged under the local symmetry. In the former case, DM will be produced dominantly from the $\eta \to l\psi$ mode while in the second case the only possible mode that remains is the $\eta \to \psi\psi$ one. Since these two modes have very different effective couplings, the DM phenomenology can be very different. We now discuss all these three distinguishing cases one by one.

We note that our second and third cases will involve some local symmetries which are not explicitly broken by Planck scale physics. Here we do not outline a complete model for such cases but point out the distinguishing DM phenomenology without affecting the neutrino phenomenology. The additional gauge interactions of ψ, η that can prevent coupling of ψ, η to SM leptons can also produce ψ thermally in the early Universe, in principle. However, if such mediator gauge bosons are very heavy, with masses greater than the reheat temperature after inflation, then the thermal production of such DM remains suppressed [99] and nonthermal contribution from the metastable WIMP will become more relevant. Another way is to assume very feeble gauge interactions so that they never get thermalized.

[2]Recently, another scenario was proposed where the dark matter freezes-out first with underproduced freeze-out abundance followed by the decay of a long-lived particle into dark matter, filling the deficit [80,97].

A. Case I

In this subsection we discuss the DM phenomenology in the most general way, corresponding to the symmetries and particle content of the $A_4 \times Z_4$ model discussed before. As mentioned earlier, the Planck scale suppressed operators open up several decay modes of the Z_4 sector particles, namely, η, ψ. The scalar doublet η, the metastable WIMP in our case, can have three different decay modes out of which the decay into a pair of leptons and a lepton plus DM are the dominant ones. The corresponding decay widths can be written as

$$\Gamma_{\eta\to e^- e^+} = \frac{\lambda_1^2(m_\eta^2 - 4m_e^2)}{8\pi m_\eta}\sqrt{1-\frac{4m_e^2}{m_\eta^2}}, \tag{37}$$

$$\Gamma_{\eta\to\nu\psi} = \frac{\lambda_2^2(m_\eta^2 - m_\psi^2 - m_\nu^2 - 2m_\psi m_\nu)}{8\pi m_\eta} \times \sqrt{\left(1-\frac{(m_\psi - m_\nu)^2}{m_\eta^2}\right)\left(1-\frac{(m_\psi + m_\nu)^2}{m_\eta^2}\right)}, \tag{38}$$

where, λ_1 and λ_2 can be written as $\frac{Y_1'\langle\phi_{N_i}\rangle}{M_{\rm Pl}}$ and $\frac{Y_2''\langle\phi_{N_i}\rangle}{M_{\rm Pl}}$, respectively.

However in this case, DM is also not perfectly stable as the Z_4 symmetry that protects its stability gets explicitly broken by Planck suppressed terms. As can be seen from Eq. (2), ψ can decay into the Higgs boson and leptons due to the term $Y_1''\overline{L_\alpha}\,\tilde{H}\,\psi$. To forbid this decay at tree level, we consider the DM mass to be below 1 MeV. This term also can give rise to a mixing of ψ with light neutrinos of the order

$$\sin 2\theta \approx {Y''}_1 \frac{\langle H\rangle\langle\phi_N\rangle}{M_{\rm Pl} m_\psi}, \tag{39}$$

which can be tuned appropriately in order to satisfy x-ray or gamma-ray bounds.

In this case, the metastable WIMP η not only decays to DM but also the charged lepton pairs. Though DM remains out of thermal equilibrium throughout, the charged leptons are part of the thermal bath and hence producing them from η decay can, in principle, release entropy. In that case, solving the coupled Boltzmann equations for η and ψ described earlier is insufficient and one has to consider a third equation for radiation energy density of the universe. Before going to the actual DM calculations, we first check the amount of entropy release by solving the following three coupled Boltzmann equations, namely,

$$\begin{aligned}\frac{dn_{\eta^0}}{dt} &= -3Hn_{\eta^0} - \Gamma_\eta n_{\eta^0},\\ \frac{d\rho_R}{dt} &= -4H\rho_R + \Gamma_{\eta\to l^+l^-}\rho_\eta,\\ \frac{dn_\psi}{dt} &= -3Hn_\psi + \Gamma_{\eta\to\psi\nu} n_\eta,\end{aligned} \tag{40}$$

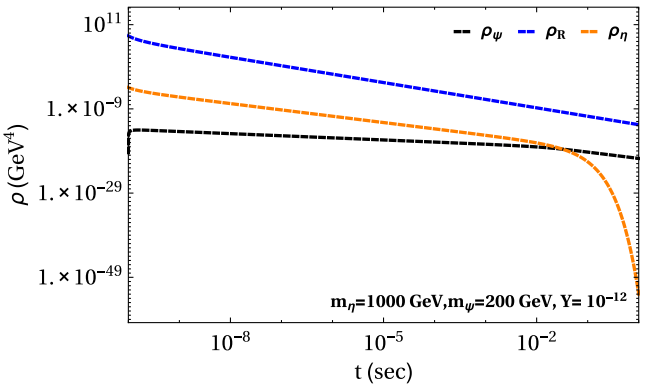

FIG. 7. The evolution of $\eta, \psi \equiv$ DM number density and radiation energy density with time for case I.

where $\Gamma_\eta = \Gamma_{\eta\to l^+l^-} + \Gamma_{\eta\to\psi\nu}$. Please note that here we are writing the Boltzmann equations in terms of ordinary number density (n), energy density (ρ), and time (t) unlike the earlier equations in terms of comoving quantities. The first equation above shows the time evolution of the number density of η where the usual dilution due to the expansion of the universe is given by the first term on the right-hand side (r.h.s.) and dilution due to the decay is given by the second term on the r.h.s.. There should, in principle, be one more term on the r.h.s., namely, $-\langle\sigma v\rangle_{\eta\eta\to pp}[n_{\eta^0}^2 - (n_{\eta^0}^{eq})^2]$ with p denoting any SM particles to which η can self annihilate into. However, we have dropped this term assuming that η has already frozen out before it starts decaying, which is a reasonable assumption (like the super-WIMP framework) for the couplings governing η decay in our model. The second and third equations are for the evolution of radiation energy density and the DM number density, respectively. Figure 7 shows that the contribution to the radiation or entropy release due to the decay of η to the lepton pairs is negligible all the way up to the epochs where η decays to reduce its number density while yielding ψ. The radiation energy density remains dominant during this and does not get any significant contribution from η decay. Since the entropy release is negligible, it thereby justifies the use of coupled Boltzmann equations only for metastable WIMP and DM in our analysis.

We now write down the coupled Boltzmann equations for η, ψ in terms of their comoving number densities as

$$\frac{dY_\eta}{dx} = -\frac{M_{\rm Pl}}{1.66}\frac{x\sqrt{g_\star(x)}}{M_{\rm sc}^2 g_s(x)}\Gamma_\eta Y_\eta, \tag{41}$$

$$\frac{dY_\psi}{dx} = \frac{M_{\rm Pl}}{1.66}\frac{x\sqrt{g_\star(x)}}{M_{\rm sc}^2 g_s(x)}\Gamma_{\eta\to\psi\bar{\nu}} Y_\eta. \tag{42}$$

We solve Eqs. (41) and (42) for different benchmark values of the parameters and show the results in Fig. 8. Since we are solving these equations after the freeze-out of metastable WIMP η, the freeze-out abundance $Y_{\eta\rm FO}$

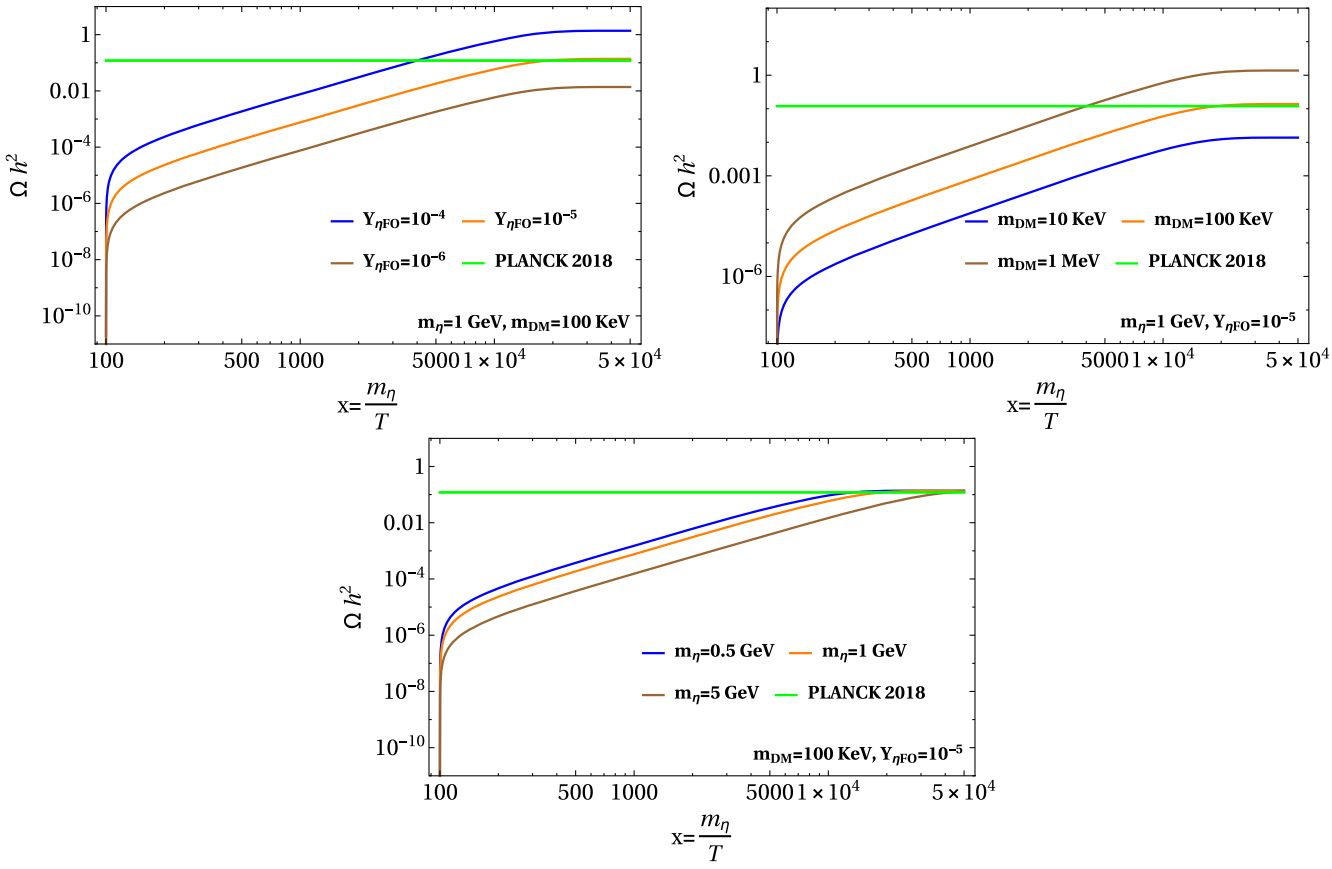

FIG. 8. Comparison of $\Omega_{\rm DM}h^2$ with respect to different model parameters for case I.

goes as input here. The left panel of the upper row in Fig. 8 shows the variation of the DM relic density as a function of temperature for different values of the freeze-out abundance of η. From the figure, it is clear that the final abundance of DM is proportional to the freeze-out abundance of η as expected. The right panel of the upper row in Fig. 8 shows the variation of DM relic density as a function of temperature for different benchmark values of DM mass by keeping the freeze-out abundance of η and mass of η fixed. As expected, the final DM relic abundance increases for an increase in DM mass. In the bottom panel plot of Fig. 8, we vary the mother particle's mass while keeping the DM mass and mother particle's freeze-out abundance fixed. We see that the final abundance of DM does not depend much upon mother particle's mass as long as the freeze-out abundance remains fixed. From these plots it is clear that the final abundance of DM ($\Omega_{\rm DM}h^2 = m_{\rm DM}Y_{\rm DM}s_0$) strictly depends on DM mass whereas it is almost independent of the mass of the mother particle. This is due to the fact that η has the same branching ratio to two different decay channels (charged lepton pairs and DM plus lepton) therefore half of its abundance is going into that of DM irrespective of its mass.

We summarize our results for case I as a scan plot shown in Fig. 9. The plot shows freeze-out abundance of η and mass of η from two different directions and requirements. The orange-blue colored band comes from the relic density requirement of DM. Since DM is being produced from η decay after thermal freeze-out of η, the orange-blue colored points give us the freeze-out abundance of η and its mass so that DM with a particular mass in that colored band has the correct relic abundance. For this plot, the effective Yukawa coupling between η and DM has been kept fixed at 10^{-12}. As can be seen, the dependence on η mass is marginal, which was also observed in the benchmark plots shown in Fig. 8. This is expected as DM abundance should strongly depend upon the freeze-out abundance of η as well as DM mass.

We then check whether the desired freeze-out abundance of η can actually be obtained for some choices of η parameters. We can write down the components of η as

$$\eta = \left(\eta^{\pm}, \frac{\eta_R + i\eta_I}{\sqrt{2}}\right)^T. \tag{43}$$

Here we consider η_R as the lightest component of η. Calculating the thermal freeze-out abundance of η_R is similar to the DM relic calculation in the inert doublet model discussed extensively in the literature [100–102]. Typically there exist two distinct mass regions, $M_\eta \leq 80$ and $M_\eta \geq 500$ GeV, where correct relic abundance criteria

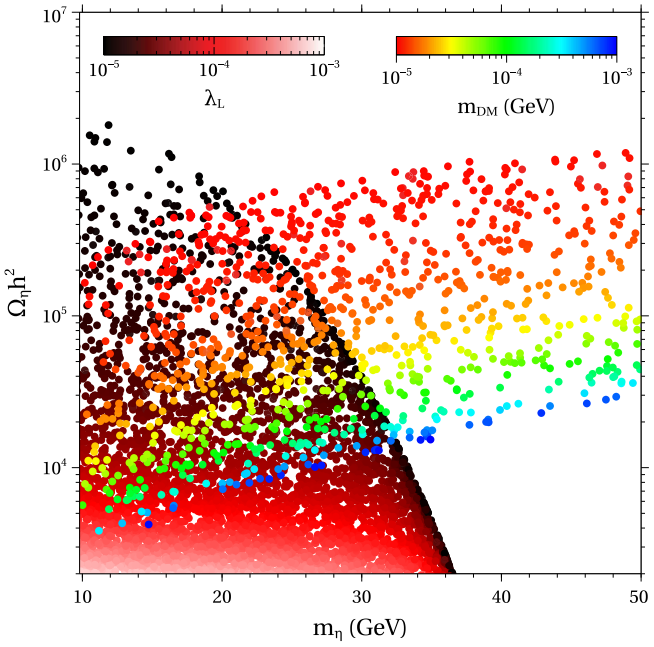

FIG. 9. Scan of model parameters for case I so that correct DM relic abundance is obtained.

can be satisfied. In both regions, depending on the mass differences $m_{\eta^\pm} - m_{\eta_R}, m_{\eta_I} - m_{\eta_R}$, the co-annihilations of η_R, $\eta^\pm$ and η_R, η_I can also contribute to the DM relic abundance [103,104]. The parameters that crucially affect the thermal freeze-out abundance of η are the mass splitting ΔM_η within the components of η and η couplings with the SM Higgs λ_L. It should be noted that there are four different Higgs doublets which can mediate η interactions with the SM particles. Here, for simplicity, we consider the scalar interactions to be mediated only by the SM like Higgs, governed by the coupling λ_L. We fix the mass splitting as $\Delta M_\eta = 50$ GeV and scan over λ_L to find the thermal freeze-out abundance of η_R. The corresponding region of parameter space is shown as the red-black color-coded region of Fig. 9. The overlapping region of orange-blue and red-black color-coded regions of Fig. 9 contain the points which satisfy the correct DM abundance criteria in our model. As can be seen from the color codes, the smaller the DM mass, the more overproduced η_R has to be, as expected. And as it is well known for freeze-out of the scalar doublet, it is the low mass regime of η_R where it is more likely to be overproduced due to the absence of sufficient annihilation channels resulting from kinematic suppression as well as departure from s-channel resonance. One can also have such an overproduced regime of η_R in the high mass limit $m_\eta \geq 1$ TeV which we have not shown in this plot.

It should be noted that there exist strong bounds on the masses of different components of η as well as their couplings with the SM Higgs. For example, precision measurements of W, Z decay widths at the LEP experiment lead to the bounds

$$m_{\eta^\pm} + m_{\eta_R} > M_{W^\pm}, \qquad m_{\eta_I} + m_{\eta_R} > M_Z,$$
$$m_{\eta^\pm} + m_{\eta_I} > M_{W^\pm}, \qquad 2m_{\eta^\pm} > M_Z.$$

The region defined by the intersection of the following conditions,

$$m_{\eta_R} < 80 \text{ GeV}, \quad m_{\eta_I} < 100 \text{ GeV}, \quad m_{\eta_I} - m_{\eta_R} > 8 \text{ GeV},$$

is also excluded from the nonobservation of dijet or dilepton signals at LEP [105,106]. The charged scalars are constrained as $m_{\eta^\pm} > 70$ GeV by reinterpreting the LEP bounds on charginos. We apply these bounds here simply by taking a conservative mass splitting $\Delta M = m_{\eta^\pm} - m_{\eta_R} = m_{\eta_I} - m_{\eta_R} = 100$ GeV in Fig. 9. Another bound comes from the LHC from the measurements of invisible decay width of the SM Higgs as well as SM Higgs decay into diphoton [106]. We check that the range of parameters we scan through satisfy these bounds.

B. Case II

In this case, η can decay only through the interaction $\frac{\langle\phi_{N_i}\rangle}{M_{\rm Pl}}\eta\bar{\nu}\psi$ as the other interaction is forbidden here. As there are no decay terms present for ψ, it is not required to consider sub-MeV mass of ψ for forbidding its decay kinematically. We consider DM mass in the GeV regime here. The relevant coupled Boltzmann equations in this case are almost the same as the ones discussed in the previous subsection, namely, Eqs. (41) and (42), except the fact that Γ_η is now replaced by $\Gamma_{\eta\to\psi\bar{\nu}}$ as there is no other decay channel present for η. They can be written as

$$\frac{dY_\eta}{dx} = -\frac{M_{\rm Pl}}{1.66}\frac{x\sqrt{g_\star(x)}}{M_{\rm sc}^2 g_s(x)}\Gamma_{\eta\to\psi\bar{\nu}}Y_\eta, \tag{44}$$

$$\frac{dY_\psi}{dx} = \frac{M_{\rm Pl}}{1.66}\frac{x\sqrt{g_\star(x)}}{M_{\rm sc}^2 g_s(x)}\Gamma_{\eta\to\psi\bar{\nu}}Y_\eta. \tag{45}$$

In Fig. 10 we have shown the variation of DM abundance as a function of $(x = \frac{m_\eta}{T})$ for different benchmark values of model parameters. The left panel of the upper row in Fig. 10 shows the variation caused by different freeze-out abundance of the mother particle while the right panel plot shows the variation with DM mass. In the lower panel plot of Fig. 10 we show the variation due to change in mother particle's mass. As in case I, the final abundance of DM does not depend much upon mother particle's mass as long as its freeze-out abundance is kept fixed. One interesting feature observed in the right panel plot in the upper row of this figure (not noticed in case I) is the change in evolution of DM density as the DM mass becomes closer to mother particle's mass. The final abundance of DM is always proportional to DM mass but when $m_{\rm DM}$ becomes very close to the m_η then η decays slowly and that can be seen

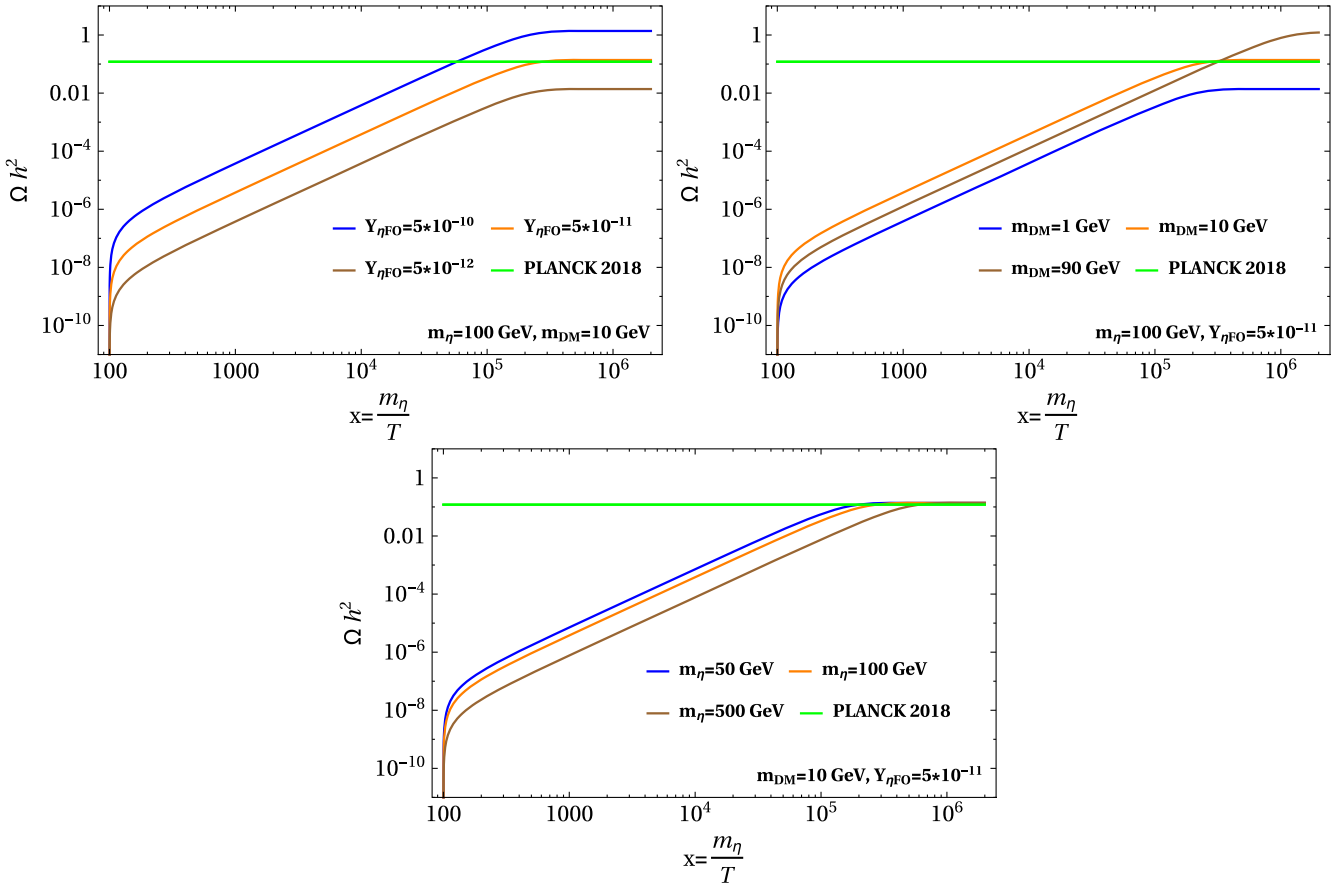

FIG. 10. Comparison of $\Omega_{\rm DM}h^2$ with respect to different model parameters for case II.

from the brown line corresponding to ($m_{\rm DM}$= 90 GeV) which grows slower with x compared to the line corresponding to lower values of DM mass ($m_{\rm DM}$= 10 GeV).

Similar to case I, here also we make a parameter scan that can give rise to the correct relic abundance of super-WIMP DM. The plot is shown in Fig. 11 where the triangles correspond to DM masses in the white-red color code while dots correspond to ΔM_η with the blue-red color code. The triangular points correspond to the parameter space that gives rise to the correct DM abundance for a particular set of $(M_{\rm DM}, M_\eta, \Omega_\eta h^2)$. As before, the mass of η does not play much role on DM abundance. However, ΔM_η plays a crucial role in generating the required freeze-out abundance of η. As can be seen from this plot, there exist very small overlaps between triangles and dots that correspond to correct DM abundance as well as realistic freeze-out abundance of the mother particle for a particular choice of ΔM_η. Thus, case II gets more constrained compared to case I in terms of final parameter space.

C. Case III

We finally consider the case where the mother particle can decay into DM only through interactions of type $\tilde{Y}_1 \frac{\langle H\rangle}{M_{\rm Pl}} \eta^\dagger \psi\psi$. This differs from case II by the facts (i) the mother particle decays into two DM particles instead of one, (ii) the effective strength of the vertex $\eta-\psi-\psi$ is much weaker $Y_{\rm eff} \approx \tilde{Y}_1 10^{-17}$. The relevant Boltzmann equations are

$$\frac{dY_\eta}{dx} = -\frac{M_{\rm Pl}}{1.66}\frac{x\sqrt{g_\star(x)}}{M_{\rm sc}^2 g_s(x)}\Gamma_{\eta\to\psi\bar{\psi}} Y_\eta, \tag{46}$$

$$\frac{dY_\psi}{dx} = \frac{2M_{\rm Pl}}{1.66}\frac{x\sqrt{g_\star(x)}}{M_{\rm sc}^2 g_s(x)}\Gamma_{\eta\to\psi\bar{\psi}} Y_\eta, \tag{47}$$

where the decay width $\Gamma_{\eta\to\psi\bar{\psi}}$ is given by Eq. (30). The corresponding results are shown in Fig. 12, where we show the evolution of the DM relic with temperature for different benchmark choices of model parameters. The overall evolution remains similar to that in case II (shown in Fig. 10) except for the fact that due to smaller effective Yukawa coupling between mother particle and DM, the yield in DM abundance happens at relatively lower temperatures or higher x. The parameter space scan for case III remains very similar to that for case II (shown in Fig. 11) and we skip showing it again.

It should be noted that in cases I and II, we considered the effective Yukawa coupling between η and ψ to be 10^{-12},

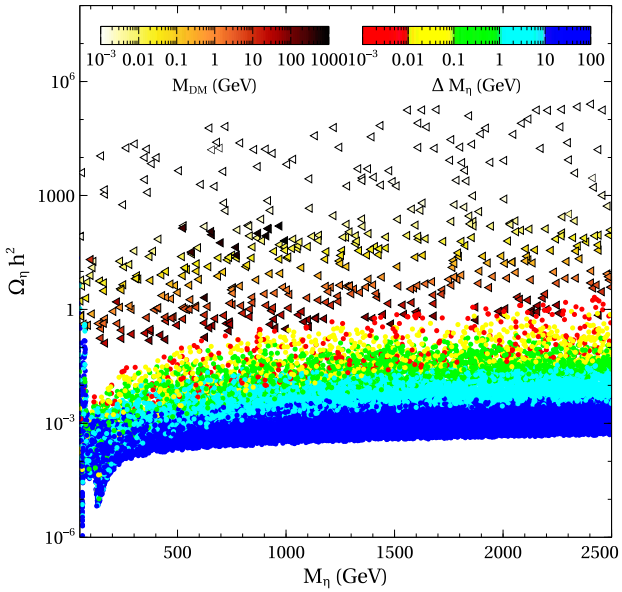

FIG. 11. Scan of model parameters for case II so that correct DM relic abundance is obtained.

which will require some fine-tuning in the Yukawa couplings appearing with the Planck suppressed operators if the scale of A_4 symmetry that is, u lies close to GUT scale. In case III, the effective Yukawa coupling is very small 10^{-16}, which arises naturally from the ratio of the electroweak scale to the Planck scale. In case III, the effective Yukawa coupling of super-WIMP is independent of the A_4 breaking scale and requires no fine-tuning. The smallness of effective Yukawa couplings chosen here also justifies the validity of super-WIMP formalism where the major nonthermal contribution to a DM relic comes after the metastable WIMP freezes out. In general, a nonthermal or FIMP dark matter scenario contribution to DM can arise while the mother particle is in thermal equilibrium as well as after the mother particle freezes out [73]. Equilibrium contribution dominates for larger Yukawa coupling $Y_{\rm eff} \sim 10^{-9}$–10^{-8} and for chosen Yukawa couplings here, the equilibrium contribution remains suppressed below 5%. This also has helped us to solve the coupled Boltzmann equations at two stages: first solving only the mother particle's equation for its thermal freeze-out and then solving the coupled Boltzmann equations for the mother particle and DM as discussed above.

Finally, we check whether the three scenarios discussed in our work could affect big bang nucleosynthesis (BBN) or cosmic microwave background (CMB), the two pillars of success of standard ΛCDM cosmology. The bounds can, in principle, be severe in case I where there is a late decay of the mother particle η into standard model leptons and dark matter. For example, if η decays into light neutrinos and

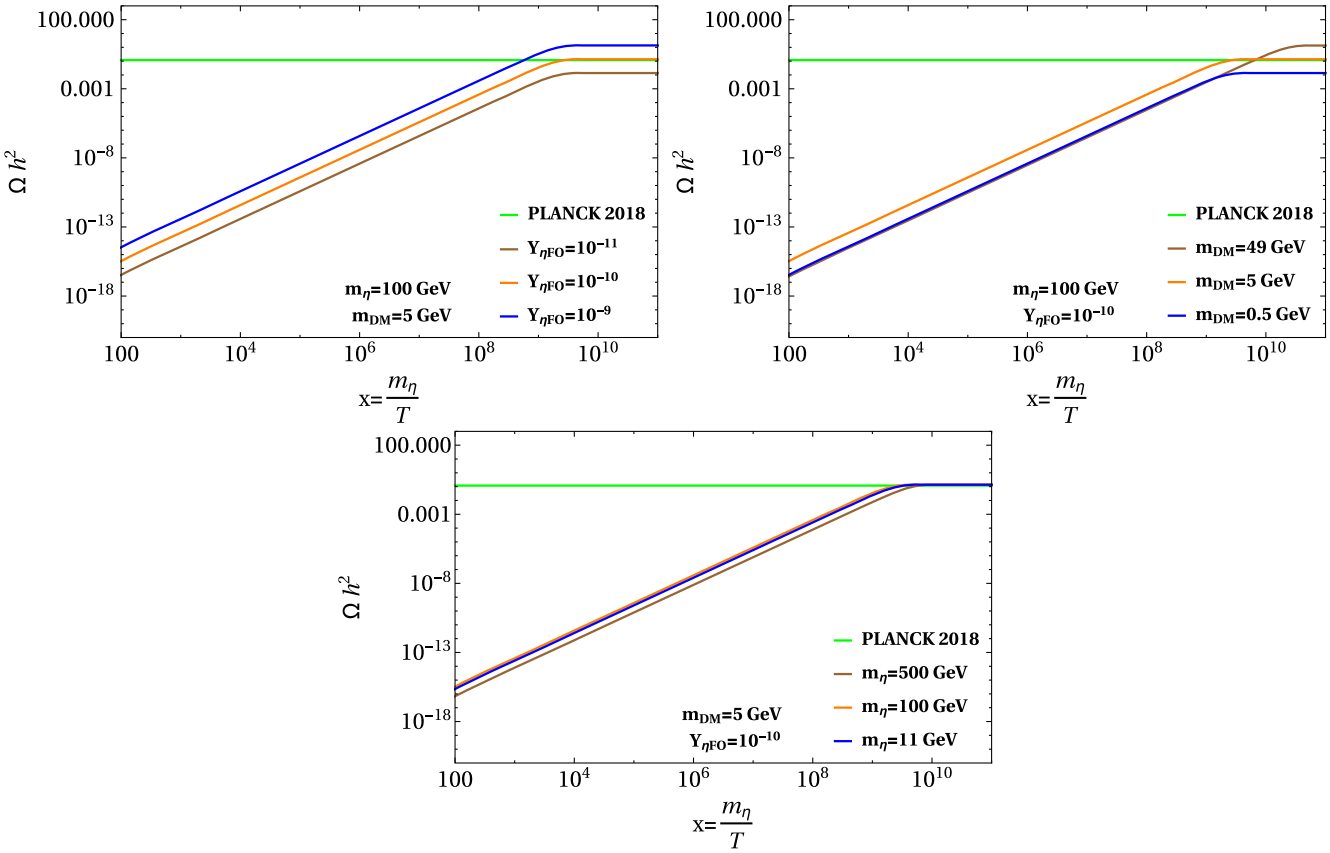

FIG. 12. Comparison of $\Omega_{\rm DM}h^2$ with respect to different model parameters for case III.

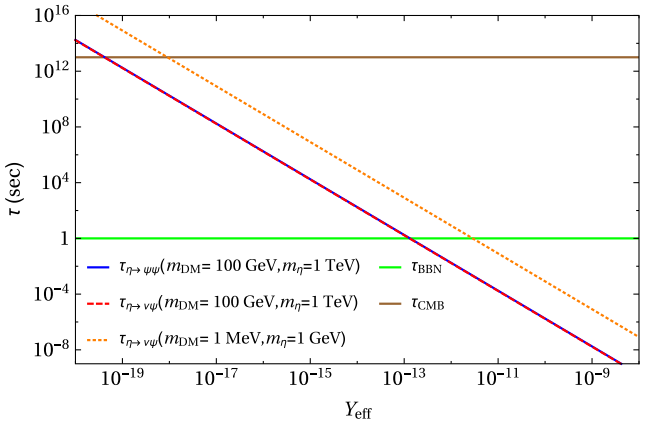

FIG. 13. Lifetime of mother particle η as a function of effective Yukawa coupling $Y_{\rm eff}$ for its two body decay into dark matter.

dark matter around the BBN epoch ($t_{\rm BBN} \sim 1$ s), it may affect the neutrino decoupling temperature, thereby affecting the successful predictions of BBN. Similarly, if the lifetime of η is more than the epoch of recombination ($t_{\rm CMB} \sim 10^{13}$ s), the CMB spectrum can be distorted. Since the CMB power spectrum is sensitive to both dark and visible matter, both case I (visible decay) as well as case II, and III (invisible decay) can affect it. We plot the lifetime of η with effective Yukawa coupling $Y_{\rm eff}$ involved in visible decay $\eta \to \nu\psi$, $\nu \equiv$ SM lepton as well as invisible decay $\eta \to \psi\psi$ and show it in Fig. 13. As can be seen from this plot, the effective Yukawa coupling of our case I $Y_{\rm eff} = 10^{-12}$ gives rise to a lifetime less than the BBN epoch keeping it safe from relevant constraints. Similarly, the Yukawa coupling of case III that is, $Y_{\rm eff} = 10^{-16}$, gives rise to a lifetime less than the recombination epoch, evading tight constraints on mass difference $\delta m = m_\eta - m_{\rm DM}$ for both visible decay [107] as well as invisible decay [108,109].

V. CONCLUSION

We have studied a scenario where light neutrino masses and mixing, at the renormalizable level, is dictated by discrete flavor symmetries based on $A_4 \times Z_4$. While the non-Abelian discrete flavor symmetry A_4 leads to TBM type light neutrino mixing for generic choices of vacuum alignments, the Z_4 symmetry dictates the dynamics of the dark sector comprising of a scalar doublet η and a singlet vectorlike fermion ψ. Clearly the renormalizable version of the model is ruled out by the observations of the nonzero reactor mixing angle θ_{13}. Also the dark sector it predicts can have an inert scalar doublet dark matter with correct relic abundance while the singlet fermion in the dark sector remains decoupled from the usual thermal bath resulting in its negligible abundance.

In order to achieve the correct neutrino phenomenology, we utilize the fact that global symmetries are conjectured to be broken explicitly at the Planck scale, possibly by gravitational effects. Such effects can mimic as Planck suppressed operators in the model which explicitly break the discrete symmetries. These corrections not only can generate nonzero θ_{13} but also changes to the dark sector dynamics. In the minimal scenario, such Planck suppressed operators can induce decay of dark sector scalar doublet η into both standard model particles as well as the dark sector singlet fermion ψ. In fact, such operators also open up decay modes of dark sector particles into the SM ones. In the minimal model, one can make ψ kinematically long-lived by going to low mass range and tuning the relevant couplings. On the other hand, the decay modes of η into ψ helps in realizing the super-WIMP mechanism where a metastable WIMP freezes-out from the thermal bath and then decays into a super-weakly interacting dark matter particle.

The tree level neutrino mass matrix originating from a type I seesaw mechanism can receive several corrections due to the Planck suppressed operators. Such corrections can arise either in the light neutrino mass matrix directly due to the Weinberg operator, in Dirac neutrino mass matrix, or heavy right-handed neutrino mass matrix out of which the first one is negligible compared to the latter ones. To illustrate the role of such corrections in a simple manner, we only take the corrections to the Dirac neutrino mass matrix and show that the corrections from Planck suppressed operators can generate the necessary deviations from TBM mixing leading to a nonzero value of θ_{13}, in agreement with observations. Owing to the specific flavor structure of the model we have a specific correlation among the mixing angles appearing in the lepton mixing matrix. Such correlations can be tested in future neutrino oscillation experiments like DUNE, T2HK, etc. [110,111]. However a detailed study in this direction is beyond the scope of our present study. We also outline the super-WIMP dark matter phenomenology by considering three distinct scenario: (i) η decays to SM particles as well as ψ and ψ is kinematically long-lived, (ii) η decays to ψ and a SM neutrino while ψ is perfectly stable, (iii) η decays into a pair of ψ while ψ is perfectly stable. Out of these, the first scenario corresponds to the model that we have discussed in our work while the latter two scenarios can be realized if the discrete Z_4 symmetry in the dark sector can be uplifted to a gauge symmetry that does not get broken by gravity effects. While we do not discuss such UV complete gauge symmetric realization of Z_4 symmetry, we outline the interesting differences for super-WIMP phenomenology. The analysis for the neutrino sector in all three DM scenarios remains the same, however.

We show that correct dark matter relic abundance can be obtained in all three distinct scenarios. While direct detection of super-WIMP dark matter itself may not be very optimistic, the mother particle η can be probed at ongoing experiments. Since the lightest component of η decays to DM as well as SM leptons (in case I) with very feeble couplings, one can probe them in colliders either as missing energy or displaced vertex, long charged tracks depending upon the lifetime.

If the charged component of η is the lightest component of η then for typical super-WIMP couplings discussed in this work, it will give rise to a long charged track in colliders as its decay length will be much larger than the typical displaced vertex ones searched for. For more discussions on displaced vertex and disappearing charged track signatures of a similar model, please refer to a recent work [112]. Apart from signatures of the mother particle, the DM itself can leave some detectable signatures, especially in case I where it is not perfectly stable but long-lived. For example, a 7 keV long-lived fermion DM[3] can decay into a photon and light neutrino at the radiative level with W boson and charged leptons of the SM in loop. The corresponding decay width is given by [114]

$$\Gamma(\psi \to \nu\gamma) \approx 1.38 \times 10^{-29}\ \mathrm{s}^{-1} \left(\frac{\sin^2 2\theta}{1 \times 10^{-7}}\right) \left(\frac{M_\psi}{1\ \mathrm{keV}}\right)^5, \tag{48}$$

where θ denotes the mixing between N_1 and ν. From the observation of the 3.55 keV line, which can arise from the decay of a 7.1 keV sterile neutrino DM, the mixing angle which is in agreement with the observed flux is $\sin^2 2\theta \approx 7 \times 10^{-11}$ [115]. Such a mixing angle can be naturally obtained in the model, as seen from the expression for the mixing angle given in Eq. (39). Although the analysis of the preliminary data collected by the Hitomi satellite (before its unfortunate crash) do not confirm such a monochromatic line [116], one still needs to wait for a more sensitive observation with future experiments to have a final word on it. We leave a more detailed study of detection prospects as well as UV complete realizations of cases II and III to future works.

ACKNOWLEDGMENTS

D. B. acknowledges support from the IIT Guwahati start-up grant (reference No. xPHYSUGI-ITG01152xxDB001), Early Career Research Award from DST-SERB, Government of India (reference No. ECR/2017/001873), and Associateship Programme of Inter University Centre for Astronomy and Astrophysics (IUCAA), Pune. D. B. is also grateful to the Mainz Institute for Theoretical Physics (MITP) of the DFG Cluster of Excellence PRISMA$^+$ (Project ID 39083149), for its hospitality and its partial support during the completion of this work. D. N. would like to thank Anirban Biswas for useful discussions.

APPENDIX: A_4 MULTIPLICATION RULES

The non-Abelian discrete group A_4, also the symmetry group of a tetrahedron, is a group of even permutations of four objects. This group has four irreducible representations out of which three are one-dimensional and one three dimensional, denoted by $\mathbf{1}$, $\mathbf{1'}$, $\mathbf{1''}$, and $\mathbf{3}$, respectively, being consistent with the sum of the square of the dimensions $\sum_i n_i^2 = 12$. We denote a generic permutation $(1,2,3,4) \to (n_1, n_2, n_3, n_4)$ simply by $(n_1 n_2 n_3 n_4)$. The group A_4 can be generated by two basic permutations S and T given by $S = (4321), T = (2314)$. This satisfies

$$S^2 = T^3 = (ST)^3 = 1,$$

which is called a presentation of the group. Their product rules of the irreducible representations are given as

$$\begin{aligned}
\mathbf{1} \otimes \mathbf{1} &= \mathbf{1}, \\
\mathbf{1'} \otimes \mathbf{1'} &= \mathbf{1''}, \\
\mathbf{1'} \otimes \mathbf{1''} &= \mathbf{1}, \\
\mathbf{1''} \otimes \mathbf{1''} &= \mathbf{1'}, \\
\mathbf{3} \otimes \mathbf{3} &= \mathbf{1} \otimes \mathbf{1'} \otimes \mathbf{1''} \otimes \mathbf{3_a} \otimes \mathbf{3_s},
\end{aligned}$$

where a and s in the subscript correspond to the antisymmetric and symmetric parts, respectively. Denoting two triplets as (a_1, b_1, c_1) and (a_2, b_2, c_2), respectively, their direct product can be decomposed into the direct sum mentioned above. In the S diagonal basis, the products are given as

$$\begin{aligned}
\mathbf{1} &\backsim \mathbf{a_1 a_2} + \mathbf{b_1 b_2} + \mathbf{c_1 c_2}, \\
\mathbf{1'} &\backsim \mathbf{a_1 a_2} + \omega^2 \mathbf{b_1 b_2} + \omega \mathbf{c_1 c_2}, \\
\mathbf{1''} &\backsim \mathbf{a_1 a_2} + \omega \mathbf{b_1 b_2} + \omega^2 \mathbf{c_1 c_2}, \\
\mathbf{3_s} &\backsim (\mathbf{b_1 c_2} + \mathbf{c_1 b_2}, \mathbf{c_1 a_2} + \mathbf{a_1 c_2}, \mathbf{a_1 b_2} + \mathbf{b_1 a_2}), \\
\mathbf{3_a} &\backsim (\mathbf{b_1 c_2} - \mathbf{c_1 b_2}, \mathbf{c_1 a_2} - \mathbf{a_1 c_2}, \mathbf{a_1 b_2} - \mathbf{b_1 a_2}).
\end{aligned}$$

In the T diagonal basis, on the other hand, they can be written as

$$\begin{aligned}
\mathbf{1} &\backsim \mathbf{a_1 a_2} + \mathbf{b_1 c_2} + \mathbf{c_1 b_2}, \\
\mathbf{1'} &\backsim \mathbf{c_1 c_2} + \mathbf{a_1 b_2} + \mathbf{b_1 a_2}, \\
\mathbf{1''} &\backsim \mathbf{b_1 b_2} + \mathbf{c_1 a_2} + \mathbf{a_1 c_2}, \\
\mathbf{3_s} &\backsim \frac{\mathbf{1}}{\mathbf{3}} (\mathbf{2 a_1 a_2} - \mathbf{b_1 c_2} - \mathbf{c_1 b_2}, \mathbf{2 c_1 c_2} - \mathbf{a_1 b_2} - \mathbf{b_1 a_2}, \\
&\qquad \mathbf{2 b_1 b_2} - \mathbf{a_1 c_2} - \mathbf{c_1 a_2}), \\
\mathbf{3_a} &\backsim \frac{\mathbf{1}}{\mathbf{2}} (\mathbf{b_1 c_2} - \mathbf{c_1 b_2}, \mathbf{a_1 b_2} - \mathbf{b_1 a_2}, \mathbf{c_1 a_2} - \mathbf{a_1 c_2}).
\end{aligned}$$

Denoting two triplets as (a_1, b_1, c_1) and (a_2, b_2, c_2), respectively, their direct product in the T diagonal basis can be decomposed into the direct sum as

[3] More details of such keV fermion dark matter can be found in a recent review [113].

$$\mathbf{1} \backsim \mathbf{a_1 a_2} + \mathbf{b_1 c_2} + \mathbf{c_1 b_2},$$
$$\mathbf{1'} \backsim \mathbf{c_1 c_2} + \mathbf{a_1 b_2} + \mathbf{b_1 a_2},$$
$$\mathbf{1''} \backsim \mathbf{b_1 b_2} + \mathbf{c_1 a_2} + \mathbf{a_1 c_2},$$
$$\mathbf{3_s} \backsim (\mathbf{2a_1 a_2 - b_1 c_2 - c_1 b_2}, \mathbf{2c_1 c_2 - a_1 b_2 - b_1 a_2}, \mathbf{2b_1 b_2 - a_1 c_2 - c_1 a_2}),$$
$$\mathbf{3_a} \backsim (\mathbf{b_1 c_2 - c_1 b_2}, \mathbf{a_1 b_2 - b_1 a_2}, \mathbf{c_1 a_2 - a_1 c_2}).$$

[1] S. Fukuda *et al.* (Super-Kamiokande Collaboration), Phys. Rev. Lett. **86**, 5656 (2001).
[2] Q. R. Ahmad *et al.* (SNO Collaboration), Phys. Rev. Lett. **89**, 011301 (2002).
[3] Q. R. Ahmad *et al.* (SNO Collaboration), Phys. Rev. Lett. **89**, 011302 (2002).
[4] S. Abe *et al.* (KamLAND Collaboration), Phys. Rev. Lett. **100**, 221803 (2008).
[5] K. Abe *et al.* (T2K Collaboration), Phys. Rev. Lett. **107**, 041801 (2011).
[6] Y. Abe *et al.* (Double Chooz Collaboration), Phys. Rev. Lett. **108**, 131801 (2012).
[7] F. P. An *et al.* (Daya Bay Collaboration), Phys. Rev. Lett. **108**, 171803 (2012).
[8] J. K. Ahn *et al.* (RENO Collaboration), Phys. Rev. Lett. **108**, 191802 (2012).
[9] P. Adamson *et al.* (MINOS Collaboration), Phys. Rev. Lett. **110**, 171801 (2013).
[10] M. Tanabashi *et al.* (Particle Data Group), Phys. Rev. D **98**, 030001 (2018).
[11] P. F. de Salas, D. V. Forero, C. A. Ternes, M. Tortola, and J. W. F. Valle, Phys. Lett. B **782**, 633 (2018).
[12] I. Esteban, M. C. Gonzalez-Garcia, A. Hernandez-Cabezudo, M. Maltoni, and T. Schwetz, J. High Energy Phys. 01 (2019) 106.
[13] N. Aghanim *et al.* (Planck Collaboration), arXiv:1807.06209.
[14] S. Weinberg, Phys. Rev. Lett. **43**, 1566 (1979).
[15] P. Minkowski, Phys. Lett. **67B**, 421 (1977).
[16] M. Gell-Mann, P. Ramond, and R. Slansky, Conf. Proc. **C790927**, 315 (1979).
[17] R. N. Mohapatra and G. Senjanovic, Phys. Rev. Lett. **44**, 912 (1980).
[18] J. Schechter and J. W. F. Valle, Phys. Rev. D **22**, 2227 (1980).
[19] Z.-z. Xing and Z.-h. Zhao, Rept. Prog. Phys. **79**, 076201 (2016).
[20] P. F. Harrison and W. G. Scott, Phys. Lett. B **535**, 163 (2002).
[21] Z.-z. Xing, Phys. Lett. B **533**, 85 (2002).
[22] P. F. Harrison and W. G. Scott, Phys. Lett. B **547**, 219 (2002).
[23] P. F. Harrison and W. G. Scott, Phys. Lett. B **557**, 76 (2003).
[24] P. F. Harrison and W. G. Scott, Phys. Lett. B **594**, 324 (2004).
[25] H. Ishimori, T. Kobayashi, H. Ohki, Y. Shimizu, H. Okada, and M. Tanimoto, Prog. Theor. Phys. Suppl. **183**, 1 (2010).
[26] W. Grimus and P. O. Ludl, J. Phys. A **45**, 233001 (2012).
[27] S. F. King and C. Luhn, Rep. Prog. Phys. **76**, 056201 (2013).
[28] G. Altarelli and F. Feruglio, Rev. Mod. Phys. **82**, 2701 (2010).
[29] E. Ma and G. Rajasekaran, Phys. Rev. D **64**, 113012 (2001).
[30] K. S. Babu, E. Ma, and J. W. F. Valle, Phys. Lett. B **552**, 207 (2003).
[31] M. Hirsch, J. C. Romao, S. Skadhauge, J. W. F. Valle, and A. Villanova del Moral, Phys. Rev. D **69**, 093006 (2004).
[32] E. Ma, Phys. Rev. D **70**, 031901 (2004).
[33] E. Ma, New J. Phys. **6**, 104 (2004).
[34] S.-L. Chen, M. Frigerio, and E. Ma, Nucl. Phys. **B724**, 423 (2005).
[35] E. Ma, Phys. Rev. D **72**, 037301 (2005).
[36] A. Zee, Phys. Lett. B **630**, 58 (2005).
[37] E. Ma, Mod. Phys. Lett. A **20**, 2601 (2005).
[38] E. Ma, Phys. Rev. D **73**, 057304 (2006).
[39] G. Altarelli and F. Feruglio, Nucl. Phys. **B741**, 215 (2006).
[40] S. K. Kang, Z.-z. Xing, and S. Zhou, Phys. Rev. D **73**, 013001 (2006).
[41] Y. Shimizu, M. Tanimoto, and A. Watanabe, Prog. Theor. Phys. **126**, 81 (2011).
[42] S. F. King and C. Luhn, J. High Energy Phys. 09 (2011) 042.
[43] S. Antusch, S. F. King, C. Luhn, and M. Spinrath, Nucl. Phys. **B856**, 328 (2012).
[44] S. F. King and C. Luhn, J. High Energy Phys. 03 (2012) 036.
[45] S. Gupta, A. S. Joshipura, and K. M. Patel, Phys. Rev. D **85**, 031903 (2012).
[46] S.-F. Ge, D. A. Dicus, and W. W. Repko, Phys. Rev. Lett. **108**, 041801 (2012).
[47] S.-F. Ge, H.-J. He, and F.-R. Yin, J. Cosmol. Astropart. Phys. 05 (2010) 017.
[48] S.-F. Ge, D. A. Dicus, and W. W. Repko, Phys. Lett. B **702**, 220 (2011).
[49] J. Liao, D. Marfatia, and K. Whisnant, Phys. Rev. D **87**, 013003 (2013).
[50] Z.-z. Xing, Phys. Lett. B **696**, 232 (2011).
[51] B. Adhikary, B. Brahmachari, A. Ghosal, E. Ma, and M. K. Parida, Phys. Lett. B **638**, 345 (2006).

[52] E. Ma and D. Wegman, Phys. Rev. Lett. **107**, 061803 (2011).
[53] G. Altarelli, F. Feruglio, L. Merlo, and E. Stamou, J. High Energy Phys. 08 (2012) 021.
[54] B. Karmakar and A. Sil, Phys. Rev. D **91**, 013004 (2015).
[55] M.-C. Chen, J. Huang, J.-M. O'Bryan, A. M. Wijangco, and F. Yu, J. High Energy Phys. 02 (2013) 021.
[56] D. Borah, Nucl. Phys. **B876**, 575 (2013).
[57] D. Borah, S. Patra, and P. Pritimita, Nucl. Phys. **B881**, 444 (2014).
[58] D. Borah, Int. J. Mod. Phys. A **29**, 1450108 (2014).
[59] M. Borah, D. Borah, M. K. Das, and S. Patra, Phys. Rev. D **90**, 095020 (2014).
[60] R. Kalita and D. Borah, Int. J. Mod. Phys. A **30**, 1550045 (2015).
[61] A. Mukherjee, D. Borah, and M. K. Das, Phys. Rev. D **96**, 015014 (2017).
[62] D. Borah, M. K. Das, and A. Mukherjee, Phys. Rev. D **97**, 115009 (2018).
[63] F. Zwicky, Helv. Phys. Acta **6**, 110 (1933); Gen. Relativ. Gravit. **41**, 207 (2009).
[64] V. C. Rubin and W. K. Ford, Jr., Astrophys. J. **159**, 379 (1970).
[65] D. Clowe, M. Bradac, A. H. Gonzalez, M. Markevitch, S. W. Randall, C. Jones, and D. Zaritsky, Astrophys. J. **648**, L109 (2006).
[66] D. S. Akerib *et al.* (LUX Collaboration), Phys. Rev. Lett. **118**, 021303 (2017).
[67] A. Tan *et al.* (PandaX-II Collaboration), Phys. Rev. Lett. **117**, 121303 (2016).
[68] X. Cui *et al.* (PandaX-II Collaboration), Phys. Rev. Lett. **119**, 181302 (2017).
[69] E. Aprile *et al.* (XENON Collaboration), Phys. Rev. Lett. **119**, 181301 (2017).
[70] E. Aprile *et al.*, Phys. Rev. Lett. **121**, 111302 (2018).
[71] F. Kahlhoefer, Int. J. Mod. Phys. A **32**, 1730006 (2017).
[72] M. L. Ahnen *et al.* (Fermi-LAT and MAGIC Collaborations), J. Cosmol. Astropart. Phys. 02 (2016) 039.
[73] L. J. Hall, K. Jedamzik, J. March-Russell, and S. M. West, J. High Energy Phys. 03 (2010) 080.
[74] N. Bernal, M. Heikinheimo, T. Tenkanen, K. Tuominen, and V. Vaskonen, Int. J. Mod. Phys. A **32**, 1730023 (2017).
[75] F. Elahi, C. Kolda, and J. Unwin, J. High Energy Phys. 03 (2015) 048.
[76] J. McDonald, J. Cosmol. Astropart. Phys. 08 (2016) 035.
[77] A. Biswas, D. Borah, and A. Dasgupta, Phys. Rev. D **99**, 015033 (2019).
[78] J. L. Feng, A. Rajaraman, and F. Takayama, Phys. Rev. D **68**, 063504 (2003).
[79] L. Lee, C. Ohm, A. Soffer, and T.-T. Yu, Prog. Part. Nucl. Phys. **106**, 210 (2019).
[80] D. Borah and A. Gupta, Phys. Rev. D **96**, 115012 (2017).
[81] D. Borah, B. Karmakar, and D. Nanda, J. Cosmol. Astropart. Phys. 07 (2018) 039.
[82] D. Borah, D. Nanda, and A. K. Saha, arXiv:1904.04840.
[83] L. F. Abbott and M. B. Wise, Nucl. Phys. **B325**, 687 (1989).
[84] R. Kallosh, A. D. Linde, D. A. Linde, and L. Susskind, Phys. Rev. D **52**, 912 (1995).
[85] S. W. Hawking, Commun. Math. Phys. **43**, 199 (1975).
[86] A. Ibarra, P. Strobl, and T. Toma, Phys. Rev. Lett. **122**, 081803 (2019).
[87] D. Borah, Phys. Rev. D **87**, 095009 (2013).
[88] F. Feruglio, C. Hagedorn, and L. Merlo, J. High Energy Phys. 03 (2010) 084.
[89] M. Holthausen and M. A. Schmidt, J. High Energy Phys. 01 (2012) 126.
[90] G. C. Branco, P. M. Ferreira, L. Lavoura, M. N. Rebelo, M. Sher, and J. P. Silva, Phys. Rep. **516**, 1 (2012).
[91] A. G. Akeroyd *et al.*, Eur. Phys. J. C **77**, 276 (2017).
[92] P. F. Harrison, D. H. Perkins, and W. G. Scott, Phys. Lett. B **530**, 167 (2002).
[93] B. Karmakar and A. Sil, Phys. Rev. D **93**, 013006 (2016).
[94] B. Karmakar and A. Sil, Phys. Rev. D **96**, 015007 (2017).
[95] D. Hernandez and A. Yu. Smirnov, Phys. Rev. D **86**, 053014 (2012).
[96] S. Bhattacharya, B. Karmakar, N. Sahu, and A. Sil, J. High Energy Phys. 05 (2017) 068.
[97] A. Biswas, D. Borah, and D. Nanda, J. Cosmol. Astropart. Phys. 09 (2018) 014.
[98] G. Belanger, F. Boudjema, A. Pukhov, and A. Semenov, Comput. Phys. Commun. **185**, 960 (2014).
[99] Y. Mambrini, K. A. Olive, J. Quevillon, and B. Zaldivar, Phys. Rev. Lett. **110**, 241306 (2013).
[100] E. Ma, Phys. Rev. D **73**, 077301 (2006).
[101] R. Barbieri, L. J. Hall, and V. S. Rychkov, Phys. Rev. D **74**, 015007 (2006).
[102] L. Lopez Honorez, E. Nezri, J. F. Oliver, and M. H. G. Tytgat, J. Cosmol. Astropart. Phys. 02 (2007) 028.
[103] K. Griest and D. Seckel, Phys. Rev. D **43**, 3191 (1991).
[104] J. Edsjo and P. Gondolo, Phys. Rev. D **56**, 1879 (1997).
[105] E. Lundstrom, M. Gustafsson, and J. Edsjo, Phys. Rev. D **79**, 035013 (2009).
[106] A. Belyaev, G. Cacciapaglia, I. P. Ivanov, F. Rojas, and M. Thomas, Phys. Rev. D **97**, 035011 (2018).
[107] F. D'Eramo and S. Profumo, Phys. Rev. Lett. **121**, 071101 (2018).
[108] K. Enqvist, S. Nadathur, T. Sekiguchi, and T. Takahashi, J. Cosmol. Astropart. Phys. 09 (2015) 067.
[109] D. Cheng, M. C. Chu, and J. Tang, J. Cosmol. Astropart. Phys. 07 (2015) 009.
[110] S. K. Agarwalla, S. S. Chatterjee, S. T. Petcov, and A. V. Titov, Eur. Phys. J. C **78**, 286 (2018).
[111] S. T. Petcov and A. V. Titov, Phys. Rev. D **97**, 115045 (2018).
[112] D. Borah, D. Nanda, N. Narendra, and N. Sahu, arXiv: 1810.12920.
[113] M. Drewes *et al.*, J. Cosmol. Astropart. Phys. 01 (2017) 025.
[114] P. B. Pal and L. Wolfenstein, Phys. Rev. D **25**, 766 (1982).
[115] E. Bulbul, M. Markevitch, A. Foster, R. K. Smith, M. Loewenstein, and S. W. Randall, Astrophys. J. **789**, 13 (2014).
[116] F. A. Aharonian *et al.* (Hitomi Collaboration), Astrophys. J. **837**, L15 (2017).